Journal of Neuroscience Research 87:1175–1184 (2009)

Characterization of CD8-positive Macrophages Infiltrating the Central Nervous System of Rats With Chronic Autoimmune Encephalomyelitis

Keiko Hiraki, Il-Kwon Park, Kuniko Kohyama, and Yoh Matsumoto*

Department of Molecular Neuropathology, Tokyo Metropolitan Institute for Neuroscience, Tokyo, Japan

$CD8^+$ macrophages appear in the central nervous system (CNS) under various pathological conditions such as trauma and ischemia. Furthermore, macrophages expressing CD8 were found in CNS lesions of chronic, but not acute, experimental autoimmune encephalomyelitis (EAE). To further characterize cells with this phenotype, we examined $CD8^+$ macrophages/monocytes in the CNS and peripheral organs during the course of acute and chronic EAE that had been induced by immunization of rats with myelin basic protein and myelin oligodendrocyte glycoprotein, respectively. Counting $CD8^+$ macrophages in CNS lesions revealed that their numbers increased reaching about 60% of total infiltrating macrophages in chronic EAE, while $CD8^+$ macrophages remained less than 5% throughout the course of acute EAE. Unexpectedly, however, higher abundance of $CD8^+$ monocytes/macrophages in the peripheral blood was found in both acute and chronic EAE. Real-time polymerase chain reaction analysis revealed no significant difference in the levels of chemokines and chemokine receptors of blood $CD8^+$ monocytes between acute and chronic EAE. mRNA expression of perforin, a cytotoxic substance, was up-regulated in $CD8^+$ monocytes compared with that of $CD8^-$ monocytes in both acute and chronic EAE. These findings suggest that activated $CD8^+$ macrophages may play a cytotoxic role in chronic EAE lesions and that cells other than $CD8^+$ monocytes/macrophages determined the difference in CNS pathology between acute and chronic EAE. Analysis of $CD8^+$ monocytes/macrophages may provide useful information to permit further dissect the pathomechanisms of multiple sclerosis and to develop effective immunotherapies against autoimmune diseases in the CNS.

Key words: experimental autoimmune encephalomyelitis; chronicity; CD8; macrophage

Multiple sclerosis (MS), which is considered to be an autoimmune disease involving the central nervous system (CNS) (Sospendra and Martin, 2005), is characterized by relapse and remission of the disease (Lublin and Reingold, 1996). In about half of all MS patients, the clinical course changes from relapsing–remitting to secondary progressive MS after 10 years (Noseworthy et al., 2000). However, little is known with regard to the pathomechanism of disease progression. In experimental settings, it is suggested that encephalitogenic T-cell activation is closely associated with disease relapse and progression because inactivation or elimination of pathogenic T cells prevented further relapse (Chen et al., 1998; Shao et al., 2003; Pryce et al., 2005). In contrast, tolerance induction to T cells failed to halt progression of a certain type of experimental autoimmune encephalomyelitis (EAE), suggesting that non-T immune cells, such as macrophages (MΦ), are involved in disease progression (Pryce et al., 2005).

MΦ are major immunocompetent cells that have multiple functions. As reviewed by Duffield (2003), MΦ in inflammatory lesions either promote immune-mediated damage or act as tissue-healing cells, depending on their subtypes, the stage of inflammation, and other undetermined factors. In vitro studies demonstrated that MΦ phagocytose degraded myelin proteins such as myelin basic protein (MBP), proteolipid protein, and myelin oligodendrocyte glycoprotein (MOG) and released tumor necrosis factor alpha (TNF-α) and nitric oxide, which may further contribute to the overall process of demyelination during MS and EAE (van der Laan et al., 1996; van der Goes et al., 2005). Recently, it was also reported that a large number of $CD8^+$ MΦ were found in the spinal cord of rats with chronic, but not acute, EAE (Schroeter et al., 2003), suggesting that $CD8^+$ MΦ play a role in the progression of EAE. Importantly, $CD8^+$ monocytes (MO)/MΦ were found in the peripheral blood of healthy human subjects and in the target

*Correspondence to: Yoh Matsumoto, Department of Molecular Neuropathology, Tokyo Metropolitan Institute for Neuroscience, Musashidai 2-6 Fuchu, Tokyo 183-8526, Japan.
E-mail: matsumoto_yo@igakuken.or.jp

Received 23 April 2008; Revised 29 June 2008; Accepted 29 August 2008

Published online 24 October 2008 in Wiley InterScience (www.interscience.wiley.com). DOI: 10.1002/jnr.21924

organ of patients with autoimmune disease (Nakamura et al., 2004; Baba et al., 2006).

In the present study, we tried to elucidate the pathomechanisms of the disease progression of chronic EAE by examining the role of $CD8^+$ MΦ that infiltrate CNS lesions. For this purpose, we first performed quantitative and longitudinal examinations of $CD8^+$ MΦ in injured spinal cord tissues. Then we measured the abundance and the kinetics of this MΦ subpopulation in the peripheral blood and lymphoid organs during EAE. Finally, we determined the levels of chemokine, chemokine receptor, and MΦ-associated factor mRNA of sorted $CD8^+$ MO in the peripheral organs in comparison with those of the $CD8^-$ counterpart. The present analysis revealed several interesting features of $CD8^+$ MΦ and strongly suggested that infiltration of $CD8^+$ MΦ into the CNS is closely associated with the maintenance of chronic lesions in the CNS.

MATERIALS AND METHODS

Unless otherwise indicated, all reagents and apparatus were obtained in Tokyo, Japan.

Animals

LEW.1AV1 rats ($RT1^{av1}$ in the LEW background gene) were provided by Dr. R. Gold, Department of Neurology, Würzburg University, Germany, and maintained in our animal facility. Lewis (LEW) rats ($RT1^l$ in the LEW background gene) were purchased from Japan SLC Inc. (Shizuoka). Rats were 8–12 weeks of age. All animal experiments were approved by the appropriate institutional committee and were performed in accordance with institutional guidelines.

Reagents

Recombinant rat MOG was prepared as described previously (Sakuma et al., 2004). Briefly, the gene coding the extracellular domain (amino acid 1–125) of MOG was amplified by using primers specific to the corresponding MOG sequence. The polymerase chain reaction (PCR) products were then digested with *Sph*I and *Hin*dIII and subcloned into pQE30 (Qiagen) used for large-scale preparation. Recombinant MOG produced in transformed *Escherichia coli* were isolated under denaturing conditions and purified with Ni-NTA Agarose (Qiagen). Then purified MOG was diluted and refolded in phosphate-buffered saline containing 1 M L-arginine, 2 mM glutathione (reduced form), and 0.2 mM glutathione (oxidized form). The obtained protein contained endotoxins at less than 10 EU/1 mg protein as determined with a Toxinometer ET-2000 (Wako). Guinea pig, bovine, and rat MBP were prepared as described previously (Deibler et al., 1972).

EAE Induction and Clinical Evaluation

In early experiments in the present study, acute EAE was induced in LEW rats by immunization with 100 μg MBP emulsified in an equal volume of complete Freund's adjuvant (CFA) (*Mycobacterium tuberculosis*, 2.5 mg/ml) in the footpads and chronic EAE was induced in LEW.1AV1 rats by immunization with 250μg MOG/CFA (*M. tuberculosis H37RA*, 2.5 mg/ml) in the tail base. Later, we learned that LEW.1AV1 rats developed acute monophasic EAE after immunization with MBP/CFA, and we also analyzed this type of EAE. Pertussis toxin (2μg) was administered intraperitoneally once at a time of MOG immunization. Clinical signs were evaluated daily as the total score of the degree of paresis of each limb and tail (partial paresis, 0.5; complete paresis, 1.0). Therefore, the clinical score of complete paralysis of four limbs plus the tail or moribund conditions was 5.

Histological and Immunohistochemical Examination

The optic nerve, cerebrum, brain stem, and cerebellum and the cervical, thoracic, and lumbar spinal cord were routinely examined for histology of chronic EAE, while acute EAE was mainly evaluated by examination of the lumbar spinal cord. The tissues were fixed in 4% paraformaldehyde and processed for paraffin embedding. Six-micron sections were cut and stained with hematoxylin and eosin (HE) and with Kruever and Barrera's (KB) method (Luxol fast blue plus cresyl violet). Inflammatory lesions were graded using sections stained with HE into four categories (grade 1, leptomeningeal and adjacent subpial cell infiltration; grade 2, mild perivascular cuffing; grade 3, extensive perivascular cuffing; grade 4, extensive perivascular cuffing and severe parenchymal cell infiltration). Demyelinating lesions were assessed using sections stained with the KB method and ED1 for MΦ into five categories (grade 1, trace of perivascular or subpial demyelination; grade 2, focal demyelination; grade 3, demyelination involving a quarter of tissues examined, i.e., the spinal tract, brain stem, cerebellar white matter or optic tract; grade 4, massive confluent demyelination involving half of the tissue; grade 5, extensive demyelination involving the entire tissues) according to Storch et al. (1998) with a few modifications.

Single immunoperoxidase staining was performed as described previously (Matsumoto and Fujiwara, 1987; Ohmori et al., 1992). Briefly, paraffin-embedded sections were deparaffinized and rehydrated. After blocking the endogenous peroxidase activity with methanol containing 0.3% hydrogen peroxide, sections were incubated with mAb ED1 (×200, purified from the hybridoma supernatant) for MΦ for 1 hr at room temperature. In the CNS, ED1 stains fine processes of microglia, whereas the whole cell bodies of MO/MΦ are positive for ED1 (our unpublished observation). Therefore, it can be said that ED1 stains mainly MΦ in diseased spinal cords. After washing, sections were incubated with biotinylated anti-mouse or rabbit IgG (×200, Vector) followed by the horseradish peroxidase–labeled Vectstain Elite ABC Kit (Vector). Horseradish peroxidase binding sites were detected in 0.005% diaminobenzidine and 0.01% hydrogen peroxide. All the procedures were performed at room temperature. To confirm the specificity of staining, primary antibodies were omitted or replaced with normal mouse IgG. The controls did not show any specific staining.

Double immunofluorescence staining was performed as follows. Frozen sections were air-dried and fixed in ether. After washing, the sections were reacted with OX8 (×200, anti-CD8 mAb), followed by incubation with Cy3-labeled anti-mouse IgG (×50, Amersham). The free binding sites of

the secondary antibody were blocked with normal mouse serum and then biotinylated ED1 was applied. Finally, the sections were incubated with Alexa 488-conjugated streptavidin (×100, Molecular Probe). Morphological observations and quantitative analysis were made by microphotographs taken under a confocal microscope (Leica).

Flow Cytometric Analysis

Leukocytes in the spleen, lymph node (LN), blood (peripheral blood leukocytes, PBL) and spinal cord were collected and stained with unlabeled OX35 (×200, anti-CD4) followed by phycoerythrin (PE)-conjugated anti-mouse IgG (×50, Vector). To saturate free binding sites of the secondary antibody, cells were incubated with normal mouse serum. Then FITC-OX42 (×20, anti-MO/MΦ mAb) and biotinylated OX8 was applied in the second step. Finally, the cells were incubated with PerCP-streptavidin (×50). During incubation (15 min each), samples were kept on ice. Ten thousand cells were analyzed in each sample by FACScan (BD Bioscience). We previously confirmed with double immunofluorescence staining that more than 95% of MO/MΦ in the lymphoid organs are positive for ED1 and OX42 (data not shown).

For the isolation of infiltrating leukocytes in the CNS, rats with or without clinical signs of EAE were killed under ether anesthesia. The spinal cords were removed and minced with scissors and treated with 0.015% collagenase/dispase (Boeringer Mannheim) and 0.015% trypsin (Sigma) for 15 min at 37°C. After passing through a stainless mesh screen, two volumes of the cell suspension were mixed with one volume of 90% Percoll solution and centrifuged at 15,000 rpm for 20 min. By means of this procedure, a myelin cake floated on the top and the infiltrating inflammatory cells were contained in the pellet. The pellet was harvested and used for analysis.

Isolation of $CD8^+$ MO/MΦ

$CD8^+$ MO/MΦ were isolated with an AutoMACS (Miltenyi Biotec) according to the manufacturer's instructions. In brief, PBL, spleen and LN cells were taken from naive or immunized rats by the density gradient methods and T, B and dendritic cells were removed by negative selection with an antibody cocktail including R73 (anti–T cells), OX33 (anti–B cells) and OX62 (anti-dendritic cells) followed by anti-mouse IgG-Microbeads (Miltenyi Biotec). Then CD4 and CD8 cell populations were negatively selected with OX8 (anti-CD8) and OX35 (anti-CD4), respectively. Finally, bead-free cells were positively selected with OX42 (anti-MO/MΦ). The purity of each population was >90%.

Real-time PCR

Total RNA was extracted from the indicated tissues with an RNAqueous Kit (Ambion) and cDNA was then synthesized by reverse transcription with a High Capacity cDNA Reverse Transcription Kit (Applied Biosystems). SYBR Green real-time PCR reactions were performed on an ABI PRISM 7500 sequence detection system (Applied Biosystems) in a total volume of 25 μl with the SYBR Premix Ex Taq (Takara Bio, Otsu, Japan). Each PCR was performed in duplicate with the following thermocycler conditions: stage 1, 95°C for 10 min for one cycle and stage 2, 95°C for 15 sec and 58°C for 1 min for 50 cycles. All primers were designed on an intron-exon junction to prevent coamplification of genomic DNA and their sequences were shown in previous reports (Matsumoto et al., 2004, 2005). Relative quantification of mRNA was performed by the standard curve method. GAPDH (glyceraldehyde-3-phosphate dehydrogenase) was used as internal control. The absence of nonspecific amplification was confirmed by dissociation curve analysis.

Statistical Analysis

Data were analyzed by Student's *t*-test or Mann-Whitney's *U*-test. *P* values less than 0.05 were considered statistically significant.

RESULTS

Clinical and Pathological Features of Acute and Chronic EAE

To characterize $CD8^+$ MΦ that appear in EAE lesions in the CNS, we induced acute EAE in LEW and LEW.1AV1 rats and chronic EAE in LEW.1AV1 rats. Figure 1 summarizes the clinical and pathological features of acute and chronic EAE. The clinical course of acute EAE was monophasic and the onset (day 10), peak (day 14), and recovery (by day 18) were relatively constant (Fig. 1A). This time course was almost identical in acute EAE induced in LEW and LEW.1AV1 rats (data not shown). In contrast, chronic EAE showed a variety of clinical courses including relapsing–remitting and secondary progressive forms as shown in our previous study (Sakuma et al., 2004). The rat depicted in Figure 1B developed clinical signs on postimmunization (PI) day 30 with remission around PI day 42, and died during severe relapse.

Routine pathology with HE and KB staining revealed that acute EAE lesions consisted mainly of small mononuclear leukocytes (Fig. 1C) with minimal demyelination (Fig. 1E), whereas there was dense and extensive "foamy macrophage" infiltration (Fig. 1D) with marked demyelination (Fig. 1F) in chronic EAE lesions. Consistent with these findings, MΦ staining with ED1 mAb revealed localized perivascular MΦ infiltration in acute EAE (Fig. 1G) and diffuse MΦ infiltration in chronic EAE (Fig. 1H).

A Large Number of $CD8^+$ MΦ Infiltrate CNS Lesions in Chronic, but Not in Acute, EAE

We then examined the presence or absence of MΦ expressing CD8 in CNS lesions at various time points of acute and chronic EAE. Acute EAE was examined on days 9 (preclinical, Fig. 2A–C), 14 (peak, Fig. 2D–F), and 21 (recovery, Fig. 2G–I). As clearly shown, the vast majority of $ED1^+$ MΦ did not express the CD8 molecule in acute EAE. Only two cells, indicated by arrows in Figure 1C and Figure 1I, were doubly labeled.

As reported previously (Schroeter et al., 2003) and confirmed here, $CD8^+$ MΦ were present in chronic

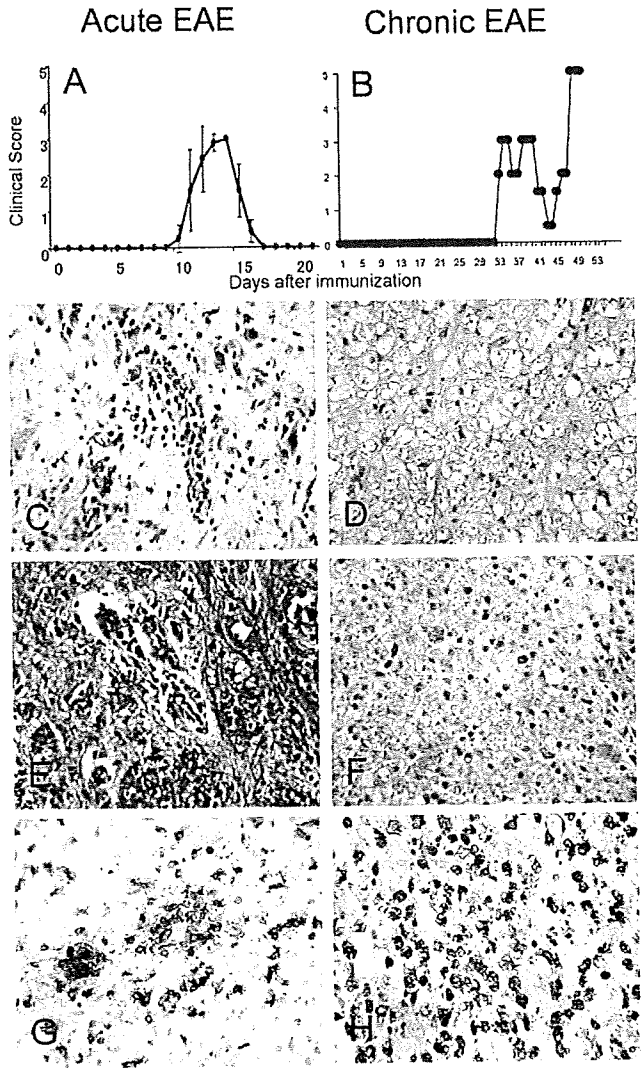

Fig. 1. Clinical and pathological features of acute and chronic EAE. LEW rats that had been immunized with MBP developed acute and monophasic EAE with a relatively constant onset and recovery (**A**). The mean clinical scores ± SD of 9 rats are shown. In contrast, chronic EAE induced by the immunization of LEW.1AV1 rats with MOG showed a variety of clinical courses including relapsing–remitting and secondary progressive EAE. The rat depicted in (**B**) developed clinical signs on PI day 30 with remission around PI day 42, and died during severe relapse. Note that the timescale in (B) is different from that in (A). Routine pathology with HE and KB staining revealed that acute EAE lesions (PI day 14) in the spinal cord consist mainly of small mononuclear leukocytes (**C**) with minimal demyelination (**E**), whereas there is dense and extensive "foamy" MΦ infiltration (**D**) with marked demyelination (**F**) in chronic EAE lesions (PI day 40) in the spinal cord. Consistent with these findings, MΦ staining with ED1 mAb revealed localized perivascular MΦ infiltration in acute EAE (**G**) and diffuse MΦ infiltration in chronic EAE (**H**). C and D, HE staining; E and F, KB staining; G and H, ED1 staining. C–H, original magnification, 120×.

EAE lesions in the spinal cord (Fig. 3). In addition to the previous study, we found an interesting finding by longitudinal examinations on days 14 (early stage, Fig. 3A–C), 20 (intermediate stage, Fig. 3D–F), and 40 (peak stage, Fig. 3G–I). On day 14, only a small number of double-positive cells were detected. Cells in yellow in Figure 3C were difficult to judge whether they were double-positive cells or simple overlap of two types of cells. However, on day 20, a definite number of MΦ expressed CD8 (Fig. 3F) and, on PI day 40, the majority of $ED1^+$ MΦ were also positive for CD8 (Fig. 3I).

Quantitative Analysis of $CD8^+ED1^+$ MΦ Infiltrating CNS Lesions in Acute and Chronic EAE

The above findings prompted us to quantitate $CD8^+$ MΦ in CNS lesions at various time points during acute and chronic EAE. As shown in Figure 4A, $CD8^+$ MΦ in acute EAE lesions (hatched bars) accounted for less than 5% throughout the course of the disease. In sharp contrast, approximately 20% of MΦ in chronic EAE lesions expressed CD8 in the early stage (solid bar on day 14). $CD8^+$ MΦ peaked on PI day 40 (58.8 ± 21.3%) and remained at a high level even on PI day 58. These findings indicate that $CD8^+$ MΦ infiltration in CNS lesions is a characteristic pathological feature of chronic EAE and that the number reaches the maximal level at the peak of chronic EAE (around PI day 40).

During analysis, we found that immunization of LEW.1AV1 rats with MBP elicited acute monophasic EAE and its clinical course was essentially the same as that found in acute EAE in LEW rats (data not shown). With spinal cord sections taken from rats with chronic EAE (LEW.1AV1-MOG in Fig. 4B) and with acute EAE (LEW.1AV1-MBP and LEW-MBP in Fig. 4B), we counted $CD8^+$ and $CD8^-$ MΦ at the indicated time points of disease. In chronic EAE, the proportion and absolute number of $CD8^+$ MΦ increased at the peak stage (day 40) compared with the early stage (day 14). The majority of MΦ forming cluster lesions expressed CD8 ("clustered" in Fig. 4B). The proportion of $CD8^+$ MΦ that did not form a cluster lesion ("nonclustered" in Fig. 4B) was relatively low compared with clustered MΦ. By contrast, in acute EAE, the proportion of $CD8^+$ MΦ in the CNS was very small (LEW-MBP). Interestingly, in LEW.1AV1 rats with acute EAE (LEW.1AV1-MBP), the proportion of $CD8^+$ MΦ was very low, as in LEW rats. These findings strongly suggest that $CD8^+$ MΦ infiltration into the CNS is closely associated with the clinical course of EAE and the used antigen but not with the rat strain.

Flow Cytometric Analysis of $CD8^+$ MΦ in the Lymphoid Organ and Peripheral Blood of Rats With Acute and Chronic EAE

Although it is generally believed that CD8 expression on MΦ occurs in CNS lesions (Popovich et al., 2003), there is no definite information regarding this

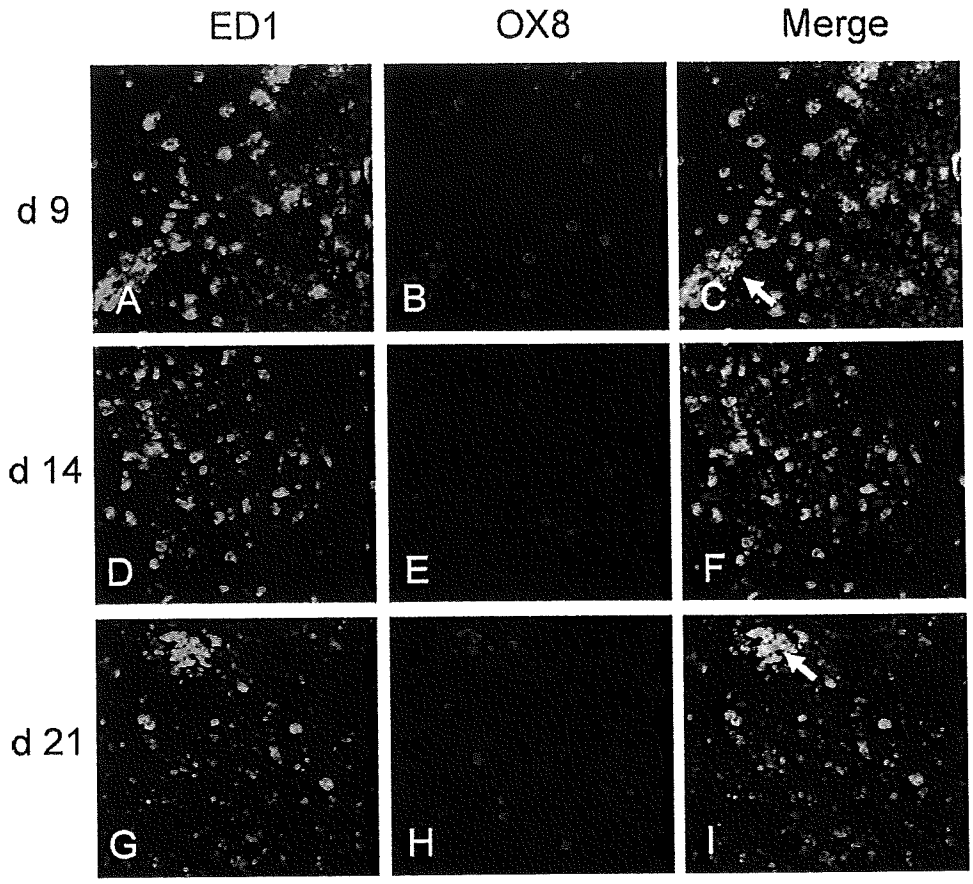

Fig. 2. Identification of $CD8^+$ MΦ in acute EAE lesions in the spinal cord. Double immunofluorescence staining for CD8 with OX8 mAb and for MΦ with ED1 mAb was performed on days 9 (**A–C**), 14 (**D–F**), and 21 (**G–I**). The majority of MΦ at all the stages examined (A,D,G) are negative for CD8 (B,E,H). Only a few cells indicated by arrows in (C) and (I) are stained positively for CD8 and EDI. Original magnification, A–I, ×200.

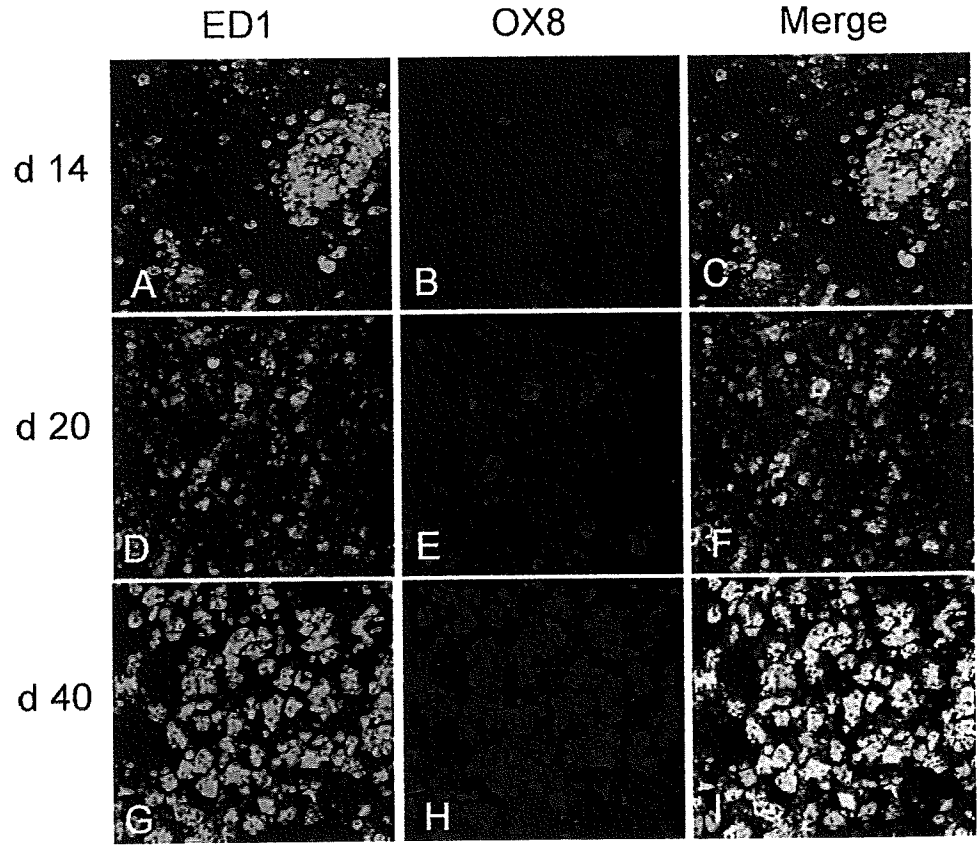

Fig. 3. Longitudinal examination of $CD8^+$ MΦ in chronic EAE lesions in the spinal cord. Double immunofluorescence staining for CD8 with OX8 mAb and for MΦ with ED1 mAb was performed on days 14 (**A–C**), 20 (**D–F**), and 40 (**G–I**). On day 14, only a small number of double-positive cells were detected. However, on day 20, a definite number of MΦ expressed CD8 (**F**) and, on day 40, the majority of $ED1^+$ MΦ were also positive for CD8 (**I**). Original magnification, A–I, ×200.

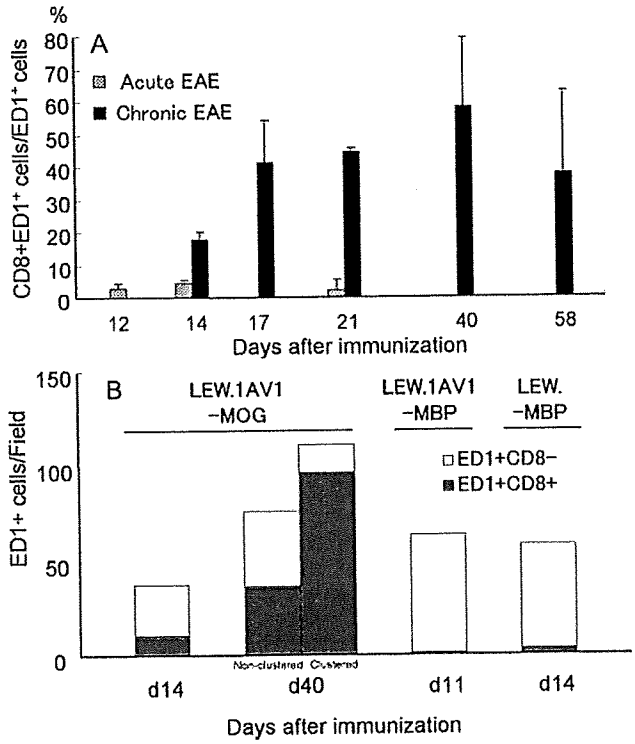

Fig. 4. (**A**) Quantitation of $CD8^+$ MΦ in acute (hatched bars) and chronic (solid bars) EAE lesions. At least three fields containing MΦ infiltration were taken as confocal images and all $ED1^+$ and $ED1^+OX8^+$ MΦ were counted and expressed as percentages ($OX8^+$ MΦ/total MΦ) ± SD. $CD8^+$ MΦ in acute EAE lesions (hatched bars) accounted for less than 5% throughout the course of the disease. In sharp contrast, approximately 20% of MΦ in chronic EAE lesions expressed CD8 in the early stage (solid bar on day 14). $CD8^+$ MΦ peaked on day 40 (58.8 ± 21.3%) and remained at a high level even on day 58. There was significant difference in the percentage of $CD8^+$ MΦ between acute and chronic EAE on days 14 and 21 ($P < 0.01$). (**B**) Comparison of the numbers of $CD8^+$ (solid bars) and $CD8^-$ (open bars) MΦ in the spinal cord at the peak of chronic (LEW.1AV1-MOG) and acute (LEW.1AV1-MBP and LEW-MBP) EAE. In chronic EAE, the proportion and absolute number of $CD8^+$ MΦ increased at the peak stage (day 40) compared with the early stage (day 14). The majority of infiltrating MΦ formed cluster lesions expressed CD8 (clustered). In contrast, the proportion of $CD8^+$ MΦ in the acute EAE lesions is very low (LEW.1AV1-MBP and LEW-MBP). The mean values ± SD for $ED1^+$ CD8- cells are 26.8 ± 7.3 (on day 14 of LEW.1AV1-MOG), 47.8 ± 17.3 (nonclustered on day 40 of LEW.1AV1-MOG), 15.3 ± 11.5 (clustered on day 40 of LEW.1AV1-MOG), 62.0 ± 29.4 (on day 11 of LEW.1AV1-MBP) and 54.5 ± 15.8 (on day 11 of LEW-MBP). At each time point, a total of four to six fields from three rats were photographed, and the mean values of the positive cells are shown.

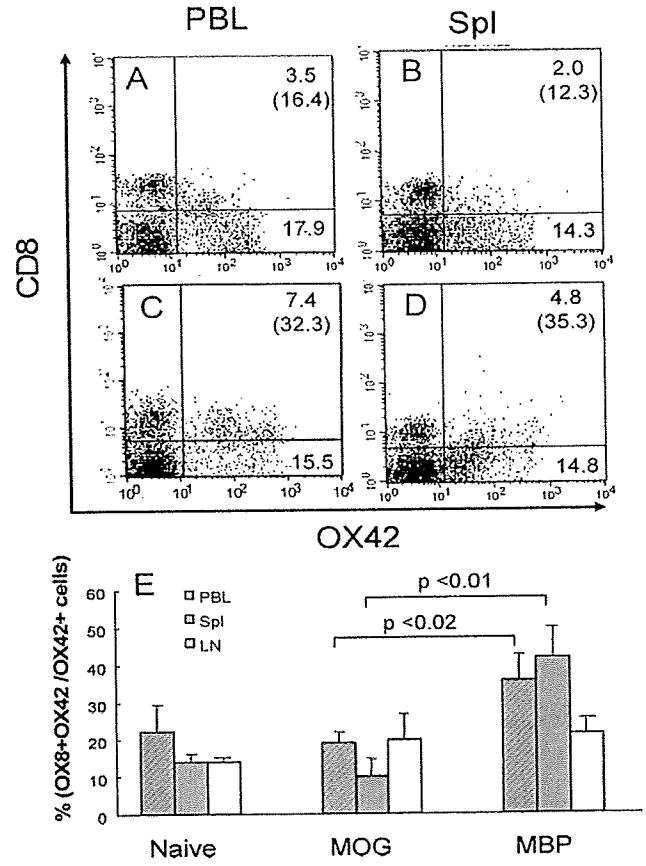

Fig. 5. **A–D:** Representative profiles of $CD8^+$ MO/MΦ in PBL (A,C) and the spleen (B,D) of MOG-immunized (A,B) (day 13) and MBP-immunized (C,D) (day 12) LEW.1AV1 rats. The numbers in parentheses are percentages of $OX8^+$ cells in total $OX42^+$ cells. **E:** In naive and MOG-immunized rats, the proportions of $CD8^+$ MO/MΦ were approximately 15–20% in PBL, spleens, and inguinal LNs. In sharp contrast, $CD8^+$ MO/MΦ in PBL and spleens of MBP-immunized rats accounted for 35% and 40%, respectively. Three rats were examined in each group, and the percentages of $OX8^+OX42^+$ cells in total $OX42^+$ cells (mean value ± SD) are shown.

issue. In order to analyze the nature of $CD8^+$ MΦ in more detail, we examined the peripheral blood, spleen, and LNs of naive, MOG-immunized and MBP-immunized LEW.1AV1 rats at the preclinical stage. In order to surface-label MΦ for flow cytometric analysis, we used OX42 for MO/MΦ instead of ED1 and OX8 for CD8. We previously confirmed by immunohistochemistry that the majority of MΦ in the lymphoid organs are double-labeled with ED1 and OX42 (data not shown). As mentioned above, immunization of LEW.1AV1 rats with MOG induced chronic EAE, whereas immunization of the same strain with MBP resulted in acute EAE. In the CNS lesions, the proportion of $CD8^+$ MΦ was high in chronic EAE and very low in acute EAE (Fig. 4B).

In lymphoid organs, a different finding was obtained. As shown in Figure 5, the proportions of $CD8^+$ MO/MΦ in naive control (Fig. 5E) and MOG-immunized (Fig. 5A,B,E) rats were approximately 15–20% in all organs examined ("Naive" and "MOG" in Fig. 5E). In sharp contrast, $CD8^+$ MO/MΦ in PBL and spleens of MBP-immunized rats (Fig. 5C–E) accounted for about 35% and 40%, respectively ("MBP" in Fig. 5E). These findings suggest that MBP immunization induces a sufficient number of

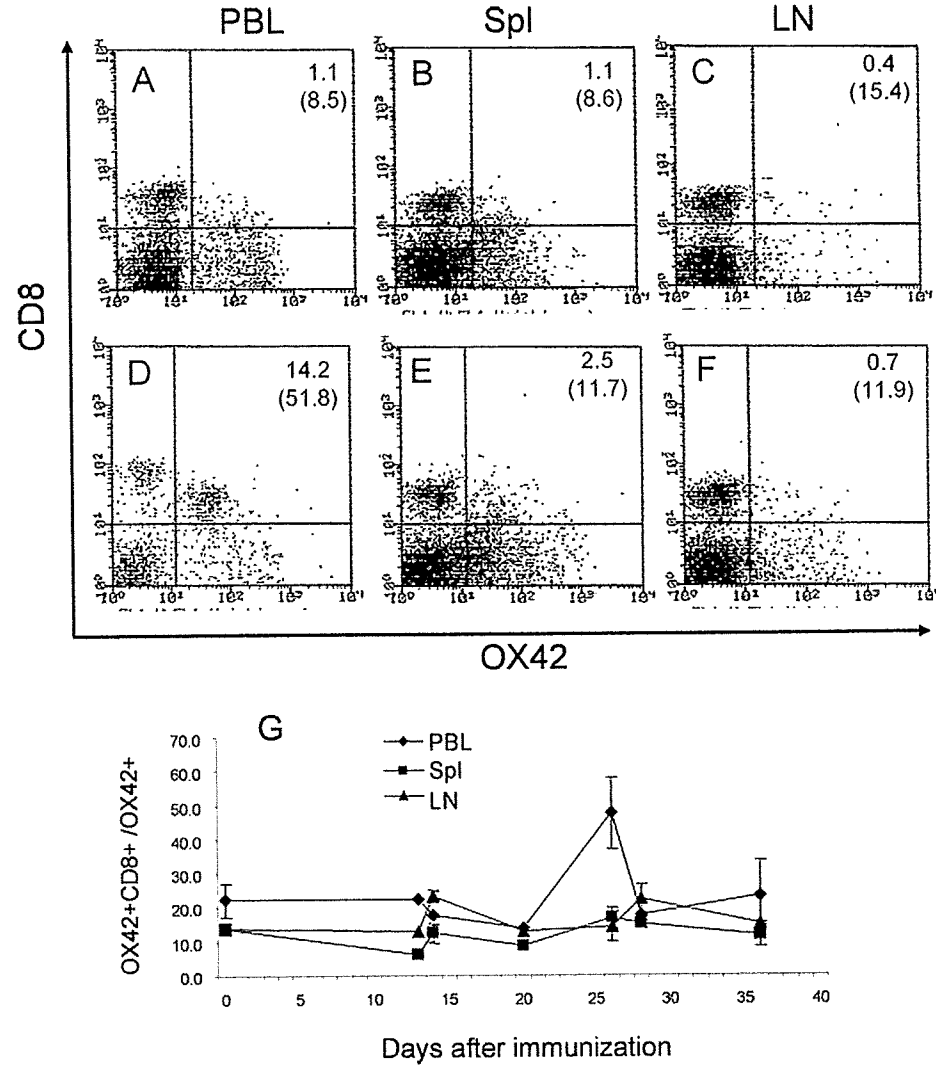

Fig. 6. **A–F:** Flow cytometric analysis of $CD8^+$ MO/MΦ in the blood, spleen, and LN of normal (**A–C**) and chronic EAE (**D–F**) LEW.1AV1 rats. PBL (**A,D**), spleen (Spl) (**B,E**), and LN (**C,F**) cells were isolated and stained for CD8 with OX8 and for MΦ with OX42. In PBL and spleen of a naive rat (A and B, respectively), $CD8^+$ MΦ accounted for 10–15%, whereas those in LN of naive rats (C) are relatively few. In a rat with chronic EAE, $CD8^+$ MO in PBL increased significantly (D), whereas those in the spleen and LNs were not significantly different from a naive rat (E,F). The numbers in parentheses are percentages of $OX8^+$ cells in total $OX42^+$ cells. **G:** During chronic EAE, the numbers of $CD8^+$ MΦ in all organs remained unchanged in the preclinical stage but $CD8^+$ MΦ abruptly increased in number around the onset of chronic EAE in PBL (D and diamonds in G). Such change was observed only in PBL and the proportion of $CD8^+$ MΦ in other organs remained stable throughout the observation period. At each time point, three to four rats were examined.

$CD8^+$ MO/MΦ in the periphery. However, MOG, but not MBP, immunization may up-regulate factors that recruit $CD8^+$ MO/MΦ into the CNS more efficiently.

We also performed similar analysis with mononuclear cells isolated from the spinal cord during the peak of chronic EAE. Unfortunately however, it was revealed that harvested $CD8^+$ cells were always small in both number and size. On the basis of this finding, we judged that the majority of foamy MΦ, the major inflammatory cell population in spinal cord lesions, were destroyed during the processes of isolation and staining for analysis and decided not to use the obtained data.

Kinetics of $CD8^+$ MΦ in the Lymphoid Organ and Peripheral Blood in Chronic EAE

Flow cytometric analysis that used PBL obtained from rats on day 12–13 revealed that the proportion of $CD8^+$ MO was significantly higher in MBP-immunized rats than in MOG-immunized rats (Fig. 5E). To examine in more detail, we made a longitudinal examination of the numbers of $CD8^+$ MO/MΦ in the periphery during the course of chronic EAE. The representative profiles of naive control rats and rats with EAE are shown in Figure 6A–F and the summary is in Figure 6G. In PBL, spleens, and LNs (Fig. 6A,B,C, respectively) of naive control rats, $CD8^+$ MO/MΦ accounted for about 10–20%. During chronic EAE, the numbers of $CD8^+$ MO/MΦ in all organs remained unchanged at the preclinical stage (Fig. 6G) but $CD8^+$ MO/MΦ in PBL abruptly increased in number around the onset of chronic EAE (Fig. 6D and diamonds in Fig. 6G). Such change was observed only in PBL and the proportions of $CD8^+$ MO/MΦ in the spleen and LN remained stable throughout the observation period. Thus, it was demonstrated that $CD8^+$ MO in PBL was equally up-regulated in both MBP- and MOG-immunized rats but

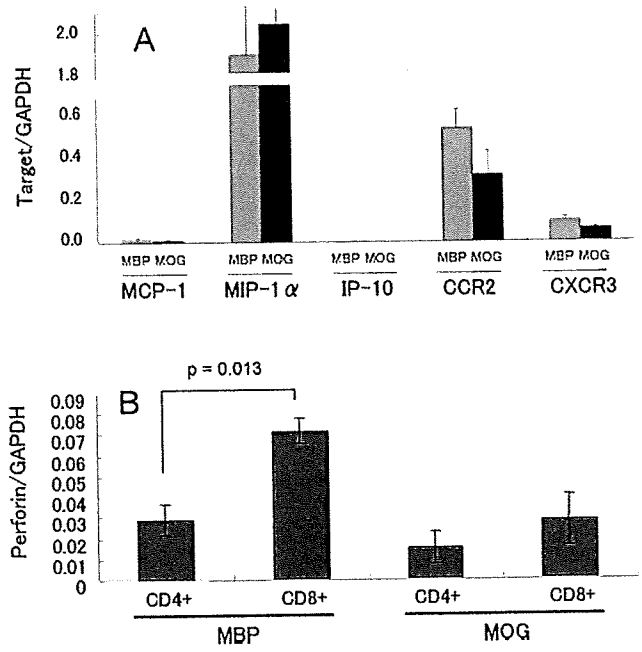

Fig. 7. Real-time PCR analysis of chemokine, chemokine receptor (**A**) and perforin (**B**) mRNA of peripheral blood MO. PBL were taken from MBP-immunized (day 12–13, grade 2.5–3, $n = 4$) and MOG-immunized (day 13–20, grade 2.5–3, $n = 4$) rats with clinical EAE. Then $CD4^+$ and $CD8^+$ MO were purified with AutoMACS. mRNA levels of the indicated molecules were determined by real-time PCR. The mRNA levels of chemokines and chemokine receptors of $CD8^+$ MO (A) and of perforin of $CD4^+$ and $CD8^+$ MO isolated from MBP- and MOG-immunized rats are shown. GAPDH was used as internal control.

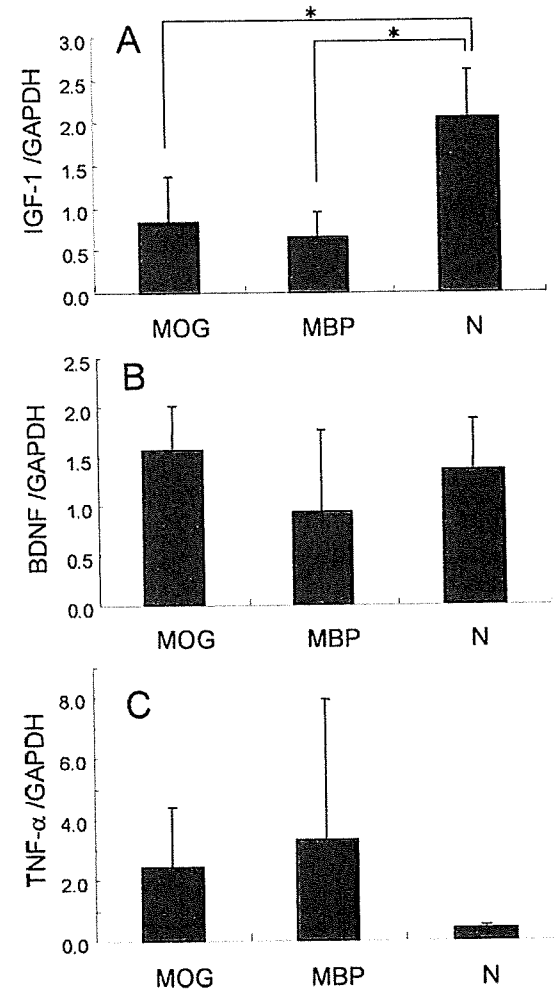

Fig. 8. Real-time PCR analysis of IGF-1 (**A**), BDNF (**B**), and TNF-α (**C**) mRNA of naive control (N) and inflamed (MOG and MBP) spinal cords. LEW.1AV1 rats were immunized with MBP or MOG, and spinal cords were taken from MBP-immunized (PI day 11, grade 4–5, $n = 3$) and MOG-immunized (day 14–20, grade 4–5, $n = 4$) rats with clinical EAE. Then mRNA levels of the indicated molecules were determined by real-time PCR. GAPDH was used as internal control. $^*P < 0.05$. There was no significant difference in TNF-α levels among three groups.

that $CD8^+$ MO/MΦ infiltrated the CNS mainly in chronic EAE.

Quantitative Analysis of Chemokines and Other Bioactive Substances by Real-time PCR

Quantitation of mRNA encoding chemokines and other bioactive substances such as perforin, granzyme B, and Fas-L was performed by using sorted cell populations of PBL. Figure 7A shows levels of chemokines and chemokine receptors in $CD8^+$ MΦ in the peripheral blood taken from MBP-immunized and MOG-immunized rats at the peak of acute and chronic EAE. Analysis revealed no significant difference between the two groups. We also examined several bioactive substances related to the cytotoxicity of $CD8^+$ MΦ and compared them with those of $CD4^+$ MΦ. As shown in Figure 7B, the perforin mRNA level was significantly higher in the CD8 population than in the CD4 population in MBP-immunized rats ($P = 0.013$), and a similar tendency was noted in MOG-immunized rats. Essentially the same results were obtained with regard to granzyme B (data not shown). However, there was no significant difference between MBP-immunized and MOG-immunized rats.

To learn the role of infiltrating MΦ in acute and chronic EAE lesions in the spinal cord, we also determined mRNA levels of tissue repair-promoting (insulin-like growth factor [IGF]-1 and brain-derived neurotrophic factor [BDNF]) and neurotoxic (TNF-α) substances (Fig. 8). IGF-1 was significantly down-regulated in both acute (MBP in Fig. 8A) and chronic (MOG in Fig. 8A) EAE lesions than in control spinal cord tissue. There was no significant difference in BDNF mRNA level among the three groups (Fig. 8B). In contrast, one of major neurotoxic substances, TNF-α, were up-regulated in both acute and chronic EAE lesions. Importantly, there was no significant difference in the levels of IGF-1, BDNF, and TNF-α between acute and chronic EAE

lesions, suggesting that it is less likely that $CD8^+$ MΦ found in chronic EAE lesions play a role in lesion repair.

DISCUSSION

It has recently become known that hematogenous MΦ bearing a unique phenotype, i.e., $CD8^+$ MΦ, infiltrate the CNS under various pathological conditions such as EAE (Schroeter et al., 2003), spinal cord injury (Popovich et al., 2003), focal ischemia (Jander et al., 1998; Schroeter et al., 2001), and Wallerian degeneration (Jander et al., 2001). Although the role of $CD8^+$ MΦ in CNS lesions is largely unknown, there are common pathological conditions. Furthermore, Schroeter et al. (2003) demonstrated that in chronic EAE, there are a large number of $CD8^+$ MΦ in the highly demyelinating lesions, whereas only small lymphocyte-like $CD8^+$ cells were found in acute EAE lesions. These findings strongly suggest that the presence of severely damaged CNS tissues is closely linked with the appearance of $CD8^+$ MΦ.

In the present study, we have extended previous studies and obtained several intriguing findings. By means of acute and chronic EAE systems, we first made longitudinal examinations of the distribution and number of $CD8^+$ MΦ in the spinal cord. Consequently, we found that $CD8^+$ MΦ in chronic EAE lesions increased in number and peaked on PI day 40. At this time point and thereafter, $CD8^+$ MΦ accounted for about 60% of total MΦ. Contrary to the previous study (Schroeter et al., 2003), a small but definite number of MΦ bearing CD8 were present in acute EAE lesions and accounted for about 5% throughout the disease course.

The kinetic study of $CD8^+$ MO/MΦ in the peripheral blood and lymphoid organ during chronic EAE revealed that there was a transient but robust increase of $CD8^+$ MO in the peripheral blood on day 26 when chronic EAE was in the early stage. This suggests that at least a part of MO acquire CD8 molecules outside the CNS and infiltrate the target organ. Although it was previously presumed that the CD8 expression by MΦ takes place in the CNS on the basis of the findings obtained by the treatment experiment with OX8 (Schroeter et al., 2001; Popovich et al., 2003), the present study clearly showed that MO expressing CD8 molecules increase in number in the blood in the early stage of chronic EAE and move into the CNS with EAE lesions. However, this finding does not exclude the possibility of CD8 molecule acquisition by MΦ in CNS lesions.

We also analyzed the numbers and percentages of $CD8^+$ MO/MΦ in the lymphoid organ and CNS with EAE lesions induced by immunization of LEW and LEW.1AV1 with MBP (acute EAE) and of LEW.1AV1 with MOG (chronic EAE). As a result, we obtained two unexpected findings. First, in the CNS lesion of LEW.1AV1 rats with acute EAE elicited by immunization with MBP, the number of infiltrating $CD8^+$ MΦ was very small compared with chronic EAE induced in the same strain. This finding clearly indicates that the appearance of $CD8^+$ MΦ in the CNS is closely associated with the type of EAE and is totally dependent on the encephalitogenic antigen used for EAE induction. Second and most unexpectedly, there were a large number of $CD8^+$ MO/MΦ in the blood of LEW.1AV1 rats with acute EAE. This suggests that, in LEW.1AV1 rats, the factors that promote the migration of $CD8^+$ MO/MΦ from the blood to the inflamed CNS are induced by MOG, but not MBP, immunization. The quantitation of chemokine and chemokine receptor mRNA by real-time PCR in the peripheral blood using sorted cell populations revealed no significant difference in the MO/MΦ phenotype between MBP-immunized and MOG-immunized rats. This finding suggests two possibilities. First, cytokines and chemokines that were not examined in the present study play a role in determining the kinetics of $CD8^+$ MO/MΦ. Second, factors produced by non-MO/MΦ, such as T and dendritic cells, are critical for the migration of $CD8^+$ MO/MΦ. In this regard, we are currently investigating more than 30 cytokines and chemokines at both protein and mRNA levels by multiplexed flow cytometric analysis.

The role of $CD8^+$ MO/MΦ is poorly understood. By means of alveolar MΦ expressing CD8, it was demonstrated that these MΦ produce TNF, IL-1β and nitric oxide after stimulation through the CD8 molecule (Hirje et al., 1998; Lin et al., 2000). Moreover, $CD8^+$ MΦ were reported to secrete perforin and granzyme B and to kill tumor cells (Baba et al., 2006, 2008). We also evaluated the function of $CD8^+$ MΦ by examining tissue repair-promoting substances such as IGF-1 and BDNF. However, we were unable to obtain the results suggesting such role. Collectively, it is possible that $CD8^+$ MΦ show strong cytotoxic effects in the CNS of rats with chronic EAE. Another important issue is related to the presence or absence of the $CD8^+$ MO/MΦ population in humans. Two groups clearly demonstrated that $CD8^+$ MO/MΦ are present in PBL of healthy subjects (Baba et al., 2006) and that a substantial number of cells with this phenotype were found in the thyroid gland of patients with autoimmune thyroid disease (Nakamura et al., 2004). Therefore, analysis of MO/MΦ with this subtype provides useful information with regard to elucidation of the pathomechanisms of MS.

In summary, we characterized the nature and kinetics of $CD8^+$ MO/MΦ during the course of acute and chronic EAE. Although $CD8^+$ MO/MΦ increased in number in the peripheral organs of rats with both acute and chronic EAE, cells with this subtype infiltrated the CNS mainly in chronic EAE. Targeting of these cells and/or the processes of their migration from the peripheral blood to the CNS could be effective immunotherapies against autoimmune diseases in the CNS.

ACKNOWLEDGMENTS

K.H. is grateful to Professor Y. Ohta, Division of Biotechnology and Life Science, Institute of Symbiotic Science and Technology, Tokyo University of Agricul-

ture and Technology, for his continuous support. This study was supported in part by Health and Labour Sciences Research Grants for Research on Psychiatric and Neurological Diseases and Mental Health and by Grants-in-Aid from the Japan Society for the Promotion of Science. Y. M. was also funded by "Health and Welfare Funds" from Tokyo Metropolitan Government.

REFERENCES

Baba T, Ishizu A, Iwasaki S, Suzuki A, Tomaru U, Ikeda H, Yoshiki T, Kasahara M. 2006. $CD4^+/CD8^+$ macrophages infiltrating at inflammatory sites: a population of monocytes/macrophages with a cytotoxic phenotype. Blood 107:2004–2012.

Baba T, Iwasaki S, Maruoka T, Suzuki A, Tomaru U, Ikeda H, Yoshiki T, Kasahara M, Ishizu A. 2008. Rat $CD4^+CD8^+$ macrophages kill tumor cells through an NKG2D- and granzyme/perforin-dependent mechanism. J Immunol 180:2999–3006.

Chen Y, Hancock WW, Marks R, Gonnella P, Weiner HL. 1998. Mechanism of recovery from experimental autoimmune encephalomyelitis: T cell depletion and immune deviation in myelin basic protein T cell receptor transgenic mice. J Neuroimmunol 82:149–159.

Deibler GE, Martenson RE, Kies MW. 1972. Large scale preparation of myelin basic protein from central nervous tissue of several mammalian species. Preparat Biochem 2:139–165.

Duffield JS. 2003. The inflammatory macrophage:a story of Jekyll and Hyde. Clin Sci 104:27–38.

Hirje N, Lin T, Bissonnette E, Belosevic M, Befus AD. 1998. Mechanisms of macrophage stimulation through CD8: macrophage $CD8^+$ and $CD8^+$ induce nitric oxide production and associated killing of the paracyte *Leishmania major*. J Immunol 160:6004–6011.

Jander S, Schroeter M, D'Urso D, Gillen C, Witte OW, Stoll G. 1998. Focal ischaemia of the rat brain elicits an unusual inflammatory response: early appearance of $CD8^+$ macrohpages/microglia. Eur J Neurosci 10:680–688.

Jander S, Lausberg F, Stoll G. 2001. Differential recruitment of $CD8^+$ macrophages during Wallerian degeneration in the peripheral and central nervous system. Brain Pathol1127–1138.

Lin T, Hirji N, Stenton GR, Gilchrist M, Grill BJ, Schreiber AD, Befus AD. 2000. Activation of macrophage CD8: pharmacological studies of TNF and IL-1β production. J Immunol 164:1783–1792.

Lublin FD, Reingold SC. 1996. Defining the clinical course of multiple sclerosis: results of an international survey. Neurology 46:907–911.

Matsumoto Y, Fujiwara M. 1987. The immunopathology of adoptively transferred experimental allergic encephalomyelitis (EAE) in Lewis rats. Part 1. Immunohistochemical examination of developing lesion of EAE. J Neurol Sci 77:35–47.

Matsumoto Y, Tsukada Y, Miyakoshi A, Sakuma H, Kohyama K. 2004. C protein-induced myocarditis and subsequent dilated cardiomyopathy: rescue from death and prevention of dilated cardiomyopathy by chemokine receptor DNA therapy. J Immunol 173:3535–3541.

Matsumoto Y, Sakuma H, Miyakoshi A, Tsukada Y, Kohyama K, Park I, Naoyuki T. 2005. Characterization of relapsing autoimmune encephalomyelitis and its treatment with decoy chemokine receptor gene. J Neuroimmunol 170:49–61.

Nakamura Y, Watanabe M, Matsuzuka F, lMaruoka H, Miyauchi A, Iwatani Y. 2004. Intrathyroidal $CD4^+$ T lymphocytes express high levels of Fas and $CD4^+CD8^+$ macrophages/dendritic cells express Fas ligand in autoimmune thyroid disease. Thyroid 14:819–824.

Noseworthy JH, Lucchinetti C, Rodriguez M, Weinshenker BG. 2000. Multiple sclerosis. N Engl J Med 343:938–952.

Ohmori K, Hong Y, Fujiwara M, Matsumoto Y. 1992. In situ demonstration of proliferating cells in the rat central nervous system during experimental autoimmune encephalomyelitis. Evidence suggesting that most infiltrating T cells do not proliferate in the target organ. Lab Invest 66:54–62.

Popovich PG, van Rooijen N, Hickey WF, Preidis G, McGaughy V. 2003. Hematogenous macrophages express CD8 and distribute to regions of lesion cavitation after spinal cord injury. Exp Neurol 182: 275–287.

Pryce G, O'Neill JK, Croxford JL, Amor S, Hankey DJ, East E, Giovannoni G, Baker D. 2005. Autoimmune tolerance eliminates relapse but fail to halt progression in a model of multiple sclerosis. J Neuroimmunol 2005:41–52.

Sakuma H, Kohyama K, Park IK, Miyakoshi A, Tanuma N, Matsumoto Y. 2004. Clinicopathological study of a myelin oligodendrocyte glycoprotein-induced demyelinating disease in LEW.1AV1 rats. Brain 127:2201–2213.

Schroeter M, Jander S, Huitinga I, Stoll G. 2001. $CD8^+$ phagocytes in focal ischemia of the rat brain: predominant origin from hematogenous macrophages and targeting to area of pannecrosis. Acta Neuropathol 101:440–448.

Schroeter M, Stoll G, Weissert R, Hartung HP, Lassmann H, Jander S. 2003. $CD8^+$ phagocyte recruitment in rat experimental autoimmune encephalomyelitis: association with inflammatory tissue destruction. Am J Pathol 163:1517–1524.

Shao H, Lei S, Sun SL, Kaplan HJ, Sun D. 2003. Conversion of monophasic to reccurent autoimmune disease by autoreactive T cell subsets. J Immunol 171:5624–5630.

Sospendra M, Martin R. 2005. Immunology of multiple sclerosis. Annu Rev Immunol 23:683–747.

Storch MK, Stefferl A, Brehm U, Weissert R, Wallstrom E, Kerschensteiner M, Olsson T, Linington C, Lassmann H. 1998. Autoimmunity to myelin oligodendrocyte glycoprotein in rats mimics the spectrum of multiple sclerosis pathology. Brain Pathol 8:681–694.

van der Goes A, Boorsma W, Hoekstra K, Montagne L, de Groot CJ, Dijkstra CD. 2005. Determination of the sequential degradation of myelin proteins by macrophages. J Neuroimmunol 161:12–20.

van der Laan LJ, Ruuls SR, Weber KS, Lodder IJ, Dopp EA, Dijkstra CD. 1996. Macrophage phagocytosis of myelin in vitro determined by flow cytometry: phagocytosis is mediated by CR3 and induces production of tumor necrosis factor-alpha and nitric oxide. J Neuroimmunol 70:145–152.

Human Molecular Genetics, 2009, Vol. 18, No. 5 942–955
doi:10.1093/hmg/ddn422
Advance Access published on December 16, 2008

Mutant SOD1 impairs axonal transport of choline acetyltransferase and acetylcholine release by sequestering KAP3

Minako Tateno[1], Shinsuke Kato[2], Takashi Sakurai[3,†], Nobuyuki Nukina[3], Ryosuke Takahashi[4] and Toshiyuki Araki[1,*]

[1]Department of Peripheral Nervous System Research, National Institute of Neuroscience, National Center of Neurology and Psychiatry, 4-1-1 Ogawa-Higashi, Kodaira, Tokyo 187-8502, Japan, [2]Department of Neuropathology, Institute of Neurological Sciences, Tottori University Faculty of Medicine, 36-1 Nishi-cho, Yonago, Tottori 683-8504, Japan, [3]Laboratory for Structural Neuropathology, RIKEN Brain Science Institute, 2-1 Hirosawa, Wako, Saitama 351-0198, Japan and [4]Department of Neurology, Kyoto University Graduate School of Medicine, 54 Kawahara-cho, Shogoin, Sakyo-ku, Kyoto 606-8507, Japan

Received September 11, 2008; Revised and Accepted December 9, 2008

Mutations in the *superoxide dismutase 1* (*sod1*) gene cause familial amyotrophic lateral sclerosis (FALS), likely due to the toxic properties of misfolded mutant SOD1 protein. Here we demonstrated that, starting from the pre-onset stage of FALS, misfolded SOD1 species associates specifically with kinesin-associated protein 3 (KAP3) in the ventral white matter of *SOD1*^{G93A}-transgenic mouse spinal cord. KAP3 is a kinesin-2 subunit responsible for binding to cargos including choline acetyltransferase (ChAT). Motor axons in *SOD1*^{G93A}-Tg mice also showed a reduction in ChAT transport from the pre-onset stage. By employing a novel FALS modeling system using NG108-15 cells, we showed that microtubule-dependent release of acetylcholine was significantly impaired by misfolded SOD1 species. Furthermore, such impairment was able to be normalized by KAP3 overexpression. KAP3 was incorporated into SOD1 aggregates in human FALS cases as well. These results suggest that KAP3 sequestration by misfolded SOD1 species and the resultant inhibition of ChAT transport play a role in the dysfunction of ALS.

INTRODUCTION

Amyotrophic lateral sclerosis (ALS) is a fatal, progressive neurodegenerative disease characterized by motor neuron cell death in the brain and spinal cord accompanied by rapid loss of muscle control and eventually complete paralysis (1,2). The vast majority of ALS cases are of a sporadic nature, while ~10% are familial (FALS). Although the cause of sporadic ALS remains unclear, 15–20% of FALS patients have point mutations in cytosolic Cu^{2+}/Zn^{2+} superoxide dismutase (SOD1). SOD1 is an antioxidant enzyme ubiquitously expressed in the cytosol, which converts the superoxide anion radical to hydrogen peroxide. More than 115 disease-causing mutations, affecting all regions of the SOD1 gene product, have been identified.

Previous studies using transgenic animal models expressing mutated human SOD1 have shown that the disease is not caused by a loss of its dismutase activity, but by the gain of toxic properties (1). Many mutant SOD1 proteins tend to become easily misfolded and form aggregates, especially under oxidative stress (3,4). Intracellular aggregates containing SOD1 were specifically detected in affected regions of both patients and animal models possessing *sod1* mutations (5–7). In spinal cords of mutant SOD1-Tg mice, misfolded intermediates of mutant SOD1 proteins, which showed a decrease in solubility and increase in size, were found prior to disease onset (8,9). These results suggest that misfolded molecules containing mutant SOD1 may contribute to motor neuron-specific damage in ALS.

*To whom correspondence should be addressed. +81 423461716; Fax: +81 423461746; Email: taraki@ncnp.go.jp
†Present address: Department of Pharmacology, Juntendo University School of Medicine. 2-1-1 Hongo, Bunkyo-ku, Tokyo, 113-8421 Japan.

Axonal transport is required for a variety of neural functions including neurotransmitter synthesis, release and recycling (10). Motor neurons often have long axons that can be more than a meter in length in humans. For this reason, orderly function of the axonal transport mechanism should be particularly important in maintaining the structure and signal transmission at the terminals of motor axons. The transport process is carried out by two major families of motor proteins, i.e. kinesin super family for anterograde transport and the cytoplasimic dynein for retrograde transport (11). Defects in axonal transport have been reported as an early sign of motor neuron diseases including ALS (12). In mutant SOD1-Tg mice, anterograde transport of neurofilaments and tubulin is partially impaired long before disease onset, presumably due to an inhibition of certain transport systems (13,14). With respect to retrograde transport, mutations in the dynein heavy chain result in motor-selective dysfunction in mice (15). Moreover, mutation in $p150^{Glued}$, a subunit of dynactin (dynein activator), was identified in a family that developed a lower motor neuron-specific disease (16). These results strongly suggest a link between the integrity of the axonal transport mechanism with the function and survival of motor neurons.

We previously studied the intracellular localization of misfolded SOD1 species by subcellular fractionation of spinal cords from *SOD1*^{G93A}-Tg mice and found a significant accumulation of misfolded SOD1 species within the axon-enriched fraction at disease onset (17). From this result, together with previous reports, we hypothesized that misfolded SOD1 species may bind to proteins required for axonal transport and thereby inhibit normal function of the motor proteins. To prove this hypothesis, we screened axonal transport-related molecules in search for proteins that associate specifically to the misfolded SOD1 species and identified KAP3 as a misfolded SOD1-interacting protein. KAP3 is a component of the kinesin-2 motor complex mediating an axonal transport of choline acetyltransferase (ChAT) in *Drosophila* (18,19). By using an *in vitro* FALS modeling system that we developed, we showed that misfolded SOD1 inhibits axonal transport-dependent release of acetylcholine (ACh). Moreover, such impairment of ACh release could be rescued by the KAP3 overexpression. This evidence strongly suggests that the sequestering of KAP3 and the resultant inhibition of ChAT transport is a novel toxic property of mutant SOD1 proteins that inevitably leads to motor neuron-specific dysfunction.

RESULTS

Misfolded SOD1 species is accumulated in ventral white matter of spinal cords in *SOD1*^{G93A}-Tg mice prior to disease onset

We previously showed by using subcellular fractionation analysis that a considerable amount of misfolded SOD1 species is located in a fraction enriched in nucleus and certain kinds of cytoskeletal proteins (i.e. glial fibrilary acidic protein and neurofilament) in *SOD1*^{G93A}-Tg mice spinal cord prior to appearance of characteristic motor symptoms of ALS (17). To analyze more detailed subcellular localization of misfolded SOD1 in spinal motor neurons of *SOD1*^{G93A}-Tg mice, we divided the spinal cord into four subsegments by laser-assisted microdissection (LMD) (summarized in Fig. 1A) and used the lysate from each segment to detect SOD1 by immunoblot analysis. Since we observed that the *SOD1*^{G93A}-Tg mice we used in this study experienced disease onset around the age of 8 months (246.5 ± 5.8 days) and died around 9.5 months (288.5 ± 7.1 days, mean $\pm$ SEM, $n = 14$), we chose to collect samples from mice of 4, 7, 8 and 9 months of age. As expected, the majority of misfolded SOD1 species (high molecular-weight bands/smears immunoreactive for SOD1) was located in the ventral gray matter at 7 months of age, which is 1 month prior to disease onset (Fig. 1B and C). At this age, we also found that a significant amount of misfolded SOD1 species was located in ventral white matter, suggesting that misfolded SOD1 species are localized in motor neuron cell bodies and their axons. We further divided the ventral white matter segment into three subsegments and confirmed a localization of misfolded SOD1 species to a motor axon-enriched segment indicated by ChAT expression (Supplementary Material, Fig. S1). Together, these results suggest that a significant amount of misfolded SOD1 species is located not only in motor neuron cell bodies, but also in motor axons of *SOD1*^{G93A}-Tg mice prior to disease onset.

Misfolded SOD1 species associates with KAP3, a kinesin-2 component

Previous reports strongly suggest that impairment of the axonal transport mechanism is linked to degeneration of motor neurons (12). Localization of misfolded SOD1 species in motor axons of *SOD1*^{G93A}-Tg mice suggests that misfolded SOD1 species may affect the function of proteins required for axonal transport. Anterograde and retrograde axonal transports are mediated by different protein complexes, which are composed of a large variety of proteins. The kinesin super family for anterograde transport, for instance, is divided into six families (kinesin-1, 2, 3, 4, 13 and 14) consisting of 45 members in human and mouse, and they associate with appropriate cargos via adaptor molecules in most cases (11). To gain more insight into the relationship between misfolded SOD1 and individual components of the molecular motor protein complex, we compared sedimentation of misfolded SOD1 in linear density gradient centrifugation with that of representative molecules that compose motor complexes in motor axon lysate. We asked whether any of these motor complex components co-migrate with misfolded SOD1. Homogenates were prepared from the ventral white matter of *SOD1*^{G93A}-Tg mice at 8 months of age (disease onset) and *SOD1*^{WT}-Tg mice expressing human wild-type *sod1* gene (non-symptomatic control) and subjected to linear Nycodenz density gradient centrifugation. SOD1 immunoreactive bands showing expected molecular weight (representing normally folded SOD1) were observed in fractions nos 1–7 in mice of both genotypes. Misfolded SOD1 species, on the other hand, were found in fractions around no. 16 only in *SOD1*^{G93A}-Tg mice. We then examined migration profiles of 17 major components of the molecular motors from five kinesin families excluding kinesin-4 which is mostly expressed in juvenile brain,

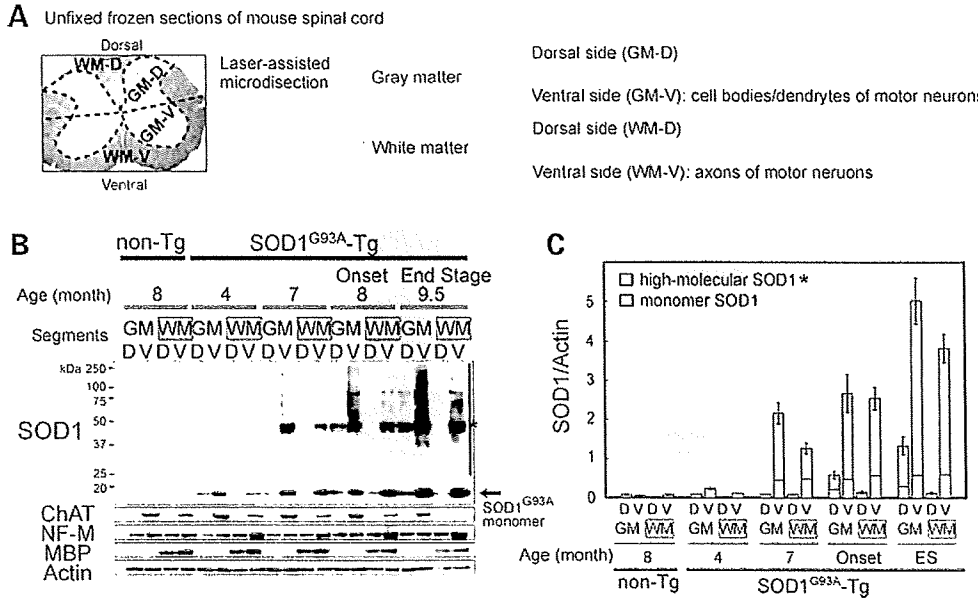

Figure 1. Misfolded SOD1 species were enriched in ventral white matter and ventral gray matter in spinal cord of *SOD1*^{G93A}-Tg mice prior to disease onset. (**A**) The procedure to divide and obtain subsegments of spinal cord is schematically shown. Unfixed frozen sections from L5 spinal cords were stained with 0.01% Toluidine blue and cut into four segments: dorsal white matter (WM-D), dorsal gray matter (GM-D), ventral white matter (WM-V) and ventral gray matter (GM-V) as indicated. (**B**) The presence of misfolded SOD1 species in the spinal cord subsegments obtained from 4, 7, 8 and 9.5 months old *SOD1*^{G93A}-Tg mice and 8 months old wild-type control (non-Tg) mice by immunoblot analysis is shown. Identity of the sample in each lane is indicated above the image. High molecular-weight bands/smears immunoreactive for SOD1 are the misfolded SOD1 species indicated by an asterisk. This misfolded SOD1 species appeared both in WM-V and GM-V of *SOD1*^{G93A}-Tg mice at 7 months. The same blot was analyzed for expression of ChAT (a motor neuron marker), neurofilament M (NF-M; a neuronal marker), MBP (a myelin marker) for controls. Actin served as a loading control. (**C**) The immunoreactivity of both monomeric (normally folded) and misfolded SOD1 that is shown in immunoblot analysis in (B) was quantified. The expression level of total SOD1 as well as monomeric and misfolded SOD1, in arbitrary units relative to actin expression is shown as a bar graph.

cytoplasmic dynein and dynactin. Among those molecules, KAP3, a subunit of the kinesin-2 motor complex, clearly co-migrated with misfolded SOD1 species around fraction no. 16 from *SOD1*^{G93A}-Tg mice (Fig. 2A, asterisks). In addition to KAP3, KIF3A and KIF3B, which are KAP3-binding partners, were weakly detected around fraction no. 16. We also observed p150^{Glued}, a dynactin subunit, co-migrated with misfolded SOD1 species. However, we did not proceed to a detailed analysis of this observation for now, because p50, another dynactin subunit (data not shown), or other dynein components such as Dynein intermediate chain (Dynein IC in Fig. 2A) did not co-migrate with misfolded SOD1 species. To confirm this association of KAP3 with misfolded SOD1, we performed immunoprecipitation analysis using the fraction nos 16 and 7. KAP3 was identified in anti-SOD1 immunoprecipitates obtained from fraction no. 16 containing misfolded SOD1 species but not in the fraction from no. 7 (Fig. 2B). In reciprocal immunoprecipitation, we found misfolded SOD1 in anti-KAP3 immunoprecipitates only in fraction no. 16. CRMP-2 (collapsin response mediator protein-2), a KAP3 counterpart for kinesin-1 motor complex, did not associate with misfolded SOD1. KAP3 seems to be associated with misfolded SOD1 species at least 2 months before disease onset, since the misfolded SOD1 species was detected in the immunoprecipitate with anti-KAP3 antibody from the extracts of 6-month-old *SOD1*^{G93A}-Tg spinal cords (Fig. 2C). Furthermore, we examined immunohistochemical localization of SOD1 and KAP3 on spinal cord sections of *SOD1*^{G93A}-Tg mice at 9 months of age (end stage). We found that protein aggregates in the remaining spinal motor neurons, immunoreactive for KAP3 were also positive for SOD1 (Fig. 2D, upper panel). The KAP3-positive aggregates also contained ubiquitin immunoreactivity, suggesting that the aggregates are cellular inclusion bodies (Fig. 2D, lower panel). These results suggest that misfolded SOD1 species specifically binds to KAP3 in motor axons of *SOD1*^{G93A}-Tg mice and that this association starts prior to the onset of motor symptoms.

Axonal transport of ChAT was significantly impaired in spinal motor neurons preceding disease onset in SOD1^{G93A}-Tg mice

Kinesin-2 is a ubiquitously and abundantly expressed molecular motor complex, which consists of KAP3 and KIF3A, together with either KIF3B or KIF3C (20). The motor domain consisting of KIF3A along with either KIF3B or KIF3C translocates along microtubules with hydrolyzing ATP, and KAP3 determines the specific cargo to be transported. Recent work using *Drosophila* ganglionic cells showed that kinesin-2 is involved in the transport of ChAT and ACh esterase (AChE) (18). Although both of the enzymes are essential for an efficient supply of ACh to the nerve terminals of spinal motor neurons, the amount of

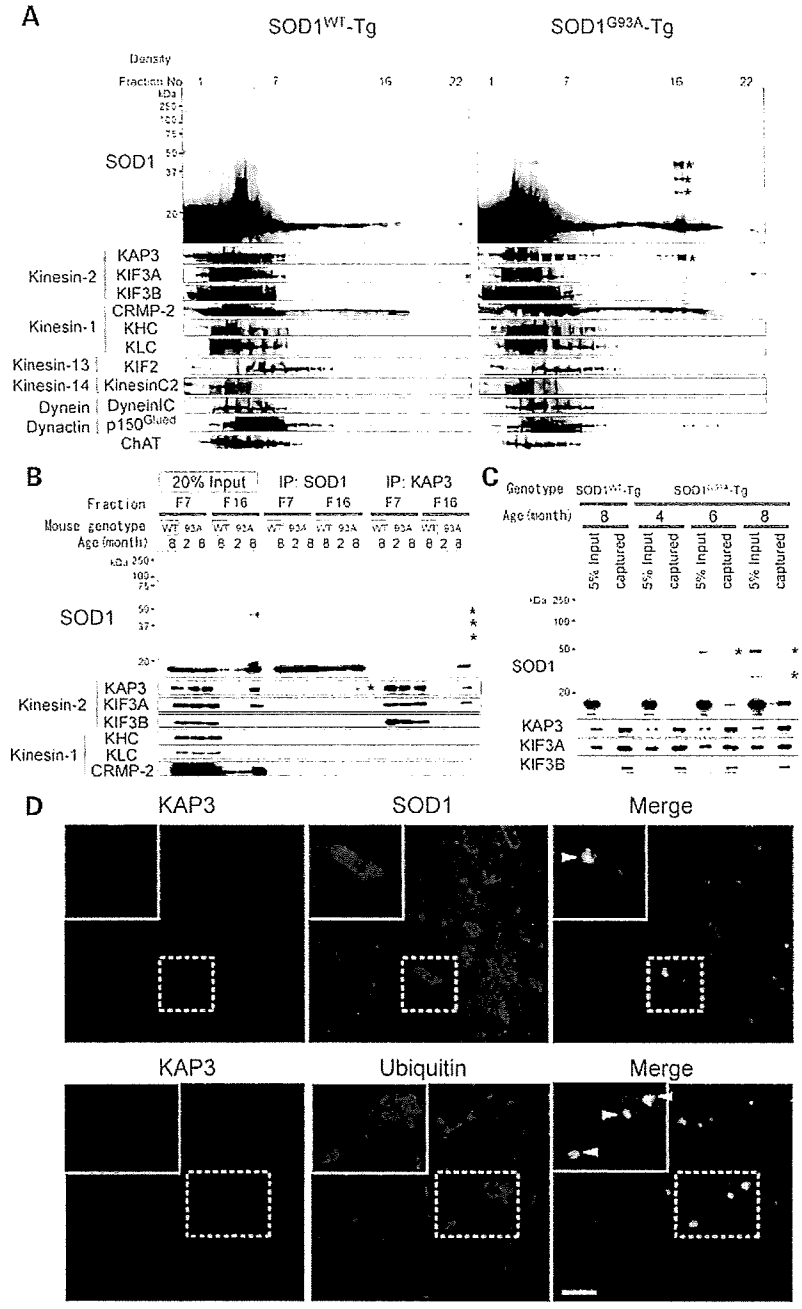

Figure 2. Misfolded SOD1 species in ventral white matter of spinal cords specifically associates with KAP3. (**A**) Fractions obtained from Nycodenz density gradient centrifugation of ventral white matter of 8-month-old *SOD1*^{WT}-Tg and *SOD1*^{G93A}-Tg spinal cords were analyzed for the presence of indicated proteins (SOD1 and individual components of kinesin and dynein motor complexes) by immunoblot analysis. Each lane (left to right) represents an aliquot collected from the top. Note that misfolded SOD1 species (indicated by asterisks) migrated around fraction no. 16 in *SOD1*^{G93A}-Tg spinal cords, where KAP3 co-migrated. (**B**) Immunoprecipitates of anti-SOD1 and KAP3 antibodies (indicated as 'IP:SOD1' or 'IP:KAP3') from Nycodenz density gradient centrifugation fractions 7 and 16 (F7, F16) of *SOD1*^{G93A}-Tg mouse spinal cords prepared above were analyzed for the presence of indicated proteins by immunoblot analysis. Also shown is an immunoblot of samples F7 and F16 (20% of the amount used for immunoprecipitation) examined for expression of the same set of proteins. Note that misfolded SOD1–KAP3 association was detected from F16 but not from F7. (**C**) Immunoprecipitates of anti-KAP3 antibody from whole spinal cord extracts of 4-, 6- and 8-month-old *SOD1*^{G93A}-Tg mice and 8-month-old *SOD1*^{WT}-Tg mice were analyzed for the presence of misfolded SOD1 by immunoblot. KIF3A and KIF3B, which are kinesin-2 components, served as controls for immunoprecipitation. Note that misfolded SOD1 species (asterisks) were captured by anti-KAP3 antibody in 6-and 8-month-old *SOD1*^{G93A}-Tg extracts. (**D**) Representative photographs of immunohistochemical co-localization of KAP3 and SOD1 (upper panel), and KAP3 and ubiquitin (lower panel) in a 9-month-old *SOD1*^{G93A}-Tg mouse spinal cord. Insets show higher magnification images of boxed area. Arrowheads indicate aggregate-like structures within motor neuron cell bodies, which were positive for both KAP3 and SOD1 (upper panel) and KAP3 and ubiquitin (lower panel). Scale bars=50 μm.

ChAT supplied is more critical for the overall production of ACh (21). Therefore, to examine the impact of misfolded SOD1–KAP3 association on the function of motor neurons in *SOD1*^{G93A}-Tg mice during the disease progression, we decided to analyze the transport of ChAT in motor neurons. To achieve this, we obtained motor–cargo protein complexes using a previously described method from ventral roots of the caudal spinal cord, which represent motor axons just extended from the spinal cords and examined the presence of ChAT by immunoblot analysis. We found that a significantly lower level of ChAT was present in cauda equina of *SOD1*^{G93A}-Tg mice compared with those of *SOD1*^{WT}-Tg at 7 months of age or later (Fig. 3A). Furthermore, kinesin-2 motor components, KAP3, KIF3A and KIF3B, all showed a similar decrease in expression during the disease progression in cauda equina of *SOD1*^{G93A}-Tg mice. On the other hand, KHC (kinesin heavy chain), KLC (kinesin light chain) (kinesin-1 components) and Rab3 (a synaptic vesicle-associated protein transported by KIF1A) were consistently expressed during the disease progression. Decreased ChAT transport in pre-symptomatic *SOD1*^{G93A}-Tg mouse sciatic nerve was also demonstrated by a ligation assay (Supplementary Material, Fig. S2A). These results suggest that the amount of ChAT transported by the kinesin-2 complex significantly decreases in motor axons of *SOD1*^{G93A}-Tg mice prior to disease onset.

The results presented in Figure 2A show that ChAT does not co-migrate with the misfolded SOD1–KAP3 complex, suggesting that KAP3 does not bind to ChAT and misfolded SOD1 at the same time. Decreased amounts of ChAT and kinesin-2 motor complex within the axons of motor neurons in *SOD1*^{G93A}-Tg mice, together with Figure 2A data, suggest that the misfolded SOD1 species may inhibit kinesin-2-mediated ChAT transportation by trapping the kinesin-2 motor complex in the motor neuron cell body and the surrounding areas. For a better understanding of the misfolded SOD1 species behavior in motor axons of *SOD1*^{G93A}-Tg mice, we compared the migration profile in a sucrose density gradient centrifugation of kinesin motor components and ChAT with that of SOD1, by using the axonal motor-cargo protein complexes prepared above as a sample. We found that a small amount of misfolded SOD1 species are present in axonal motor–cargo protein complexes and co-migrate with a small fraction of KAP3, KIF3A (Fig. 3B) and KIF3B, although the detection of KIF3B requires very long exposure (data not shown). We also found that ChAT co-immunoprecipitates with KAP3 in fractions where KAP3 and kinesin-2 components co-migrated. (Supplementary Material, Fig. S2B). These results suggest that misfolded SOD1 species not only trap the kinesin-2 motor complex via association with KAP3 in and around the cell bodies but some of the misfolded SOD1 is also transported to axons in stead of normal cargos such as ChAT.

NG108-15 cells serve as an *in vitro* model for FALS

We showed a clear correlation between the association of misfolded SOD1 with KAP3 and the inhibition of ChAT transport within *SOD1*^{G93A}-Tg mouse motor axons. To examine the causal relationship between these two phenomena in detail, we developed a novel cell culture model for FALS, in which

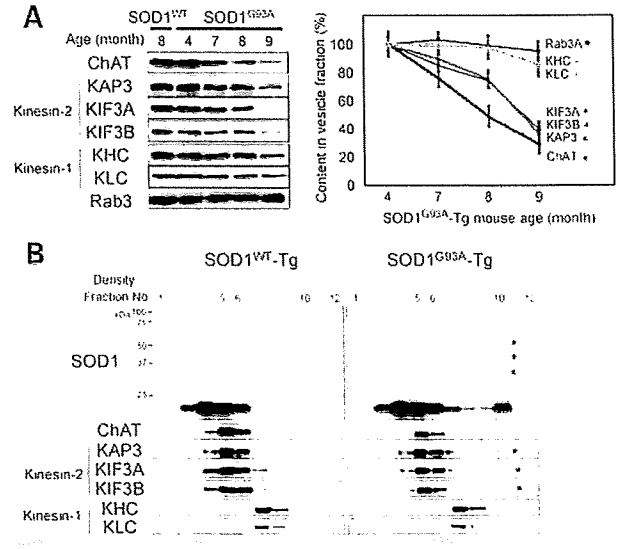

Figure 3. Axonal transport of ChAT was selectively impaired in spinal motor neurons preceding disease onset in SOD1^{G93A}-Tg mice. (**A**) Axonal transport components obtained from ventral roots from caudal spinal cords of *SOD1*^{WT}-Tg and *SOD1*^{G93A}-Tg mice at indicated ages were analyzed for the presence of indicated proteins by immunoblot analysis (left panel). The expression level of each molecule examined for *SOD1*^{G93A}-Tg mice is shown as a percentage of the level at 4 months of age (right panel). Note that the decrease in detection levels of ChAT and kinesin-2 components (KAP3, KIF3A and KIF3B) in *SOD1*^{G93A}-Tg mice became apparent at 7 months of age, 1 month before disease onset. (**B**) Fractions obtained from a sucrose density gradient centrifugation of axonal transported components from 8-month-old mice were analyzed for the presence of indicated proteins (SOD1 and individual components of kinesin motor complexes) by immunoblot analysis. Each lane (left to right) represents an aliquot collected from the top. Note that only kinesin-2 components co-migrated with misfolded SOD1 species (indicated by asterisks on the blots).

cells show cholinergic neuron-like properties—ChAT is transported within axon-like processes, ACh is released by depolarization and mutant SOD1 is misfolded/aggregated. For this purpose, we employed NG108-15 cells, which are of neuron/glia origin and known to differentiate into a cholinergic neuron-like phenotype (22,23). We first cloned a single cell-derived subline of NG108-15 cells, which we termed PNG3 (Purified NG108-15 cell-3), that showed highest expression of ChAT upon differentiation with dibutyryl cAMP and dexamethasone (data not shown). We observed that expression of ChAT and synaptophysin (an integral membrane protein found on synaptic vesicles) reaches the maximal level at ~72 h after the stimulation (Fig. 4A). By immunocytochemistry, we found that expression of ChAT and KAP3 were predominantly detected within the extended PNG3 processes in 72 h after the stimulation (Fig. 4B) as other kinesin-2 subunits (data not shown). From these observations, we decided to use PNG3 cells as a model for cholinergic neurons at day 3 after initiating differentiation for all the following experiments.

In order to use PNG3 cells as a cell line model for FALS, misfolding/aggregate formation by mutant SOD1 overexpression needs to be observed. Oxidative stress tends to cause mutant SOD1 proteins misfold and form aggregates (4). Experimentally, mutant SOD1 aggregate formation can be observed and facilitated by inhibiting proteasomal activity (24,25).

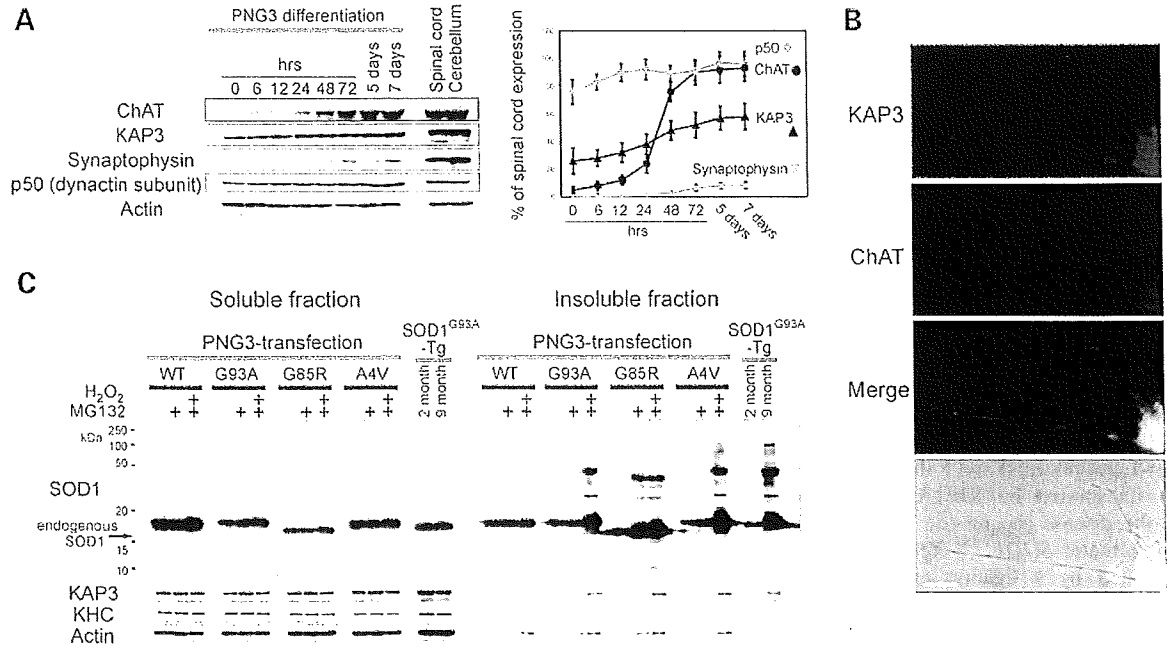

Figure 4. PNG3 cells served as an *in vitro* model system for studying mutant SOD1 toxicity on cholinergic neurons. (**A**) Expression of indicated proteins in PNG3 cells during cholinergic neuron-like differentiation was examined by immunoblot analysis. PNG3 cells were lysed at indicated times after induction of differentiation by dibutyryl cAMP and dexamethasone. Representative images of immunoblots (left panel) and quantitative analysis of the blots (right panel) are shown. Expression level is normalized to actin and relative to the level of normal spinal cord at each time point for each molecule. (**B**) Representative photographs of ChAT and KAP3 expression in differentiated PNG3 cell bodies and processes detected by immunocytochemistry are shown. Scale bar=25 μm. (**C**) Generation of misfolded SOD1 species in PNG3 cells overexpressing FLAG-tagged SOD1 bearing WT, G93A, G85R or A4V mutation was evaluated by immunoblot analysis. The transfected PNG3 cells were either untreated, treated by MG132 or treated by MG132 followed by H_2O_2 (as indicated above the images). One perecnt Triton X-100-soluble and -insoluble fractions were separately analyzed for SOD1-FLAG, KAP3, KHC and actin (for loading control). Spinal cords of 2- and 9-month-old *SOD1*^{G93A}-Tg mice were also subjected for the same set of analysis for comparison.

Therefore, we used a combined condition of increased oxidative stress plus decreased proteasomal activity to induce SOD1 misfolding and to enhance an accumulation of those misfolded SOD1 species in differentiated PNG3 cells overexpressing mutant SOD1. We transfected PNG3 cells with previously well-studied G93A, G85R and A4V mutations and wild-type control of human SOD1 for overexpression (3). Misfolded SOD1 species was detected in1% Triton X-100 insoluble fractions of lysates derived from all three types of FALS-linked SOD1 mutant transfectants but not in wild-type SOD1-overexpressing cells (Fig. 4C). We also found that SOD1 protein bearing the G85R mutation became misfolded without increasing oxidative stress, showing the previously reported unstable nature of this mutant protein (24). These results suggest that mutant SOD1 can form misfolded and/or aggregated molecules in differentiated PNG3 cells, very similar to what is seen in SOD1^{G93A}-Tg mice by pathological stresses.

For the analysis of pathological significance of misfolded SOD1–KAP3 association in this PNG3 cell model system, we next asked whether association of KAP3 with misfolded SOD1 is observed in this model just as we saw in the *SOD1*^{G93A}-Tg mice. To prove the association of KAP3 with misfolded SOD1 directly, we performed immunoprecipitation experiments using lysates of PNG3 cells transfected with either wild-type or mutant SOD1, and then treated with hydrogen peroxide to induce the mutant SOD1 misfolding. We found that anti-KAP3 immunoprecipitates contained misfolded SOD1 species, and the antibody against mutant SOD1-Flag immunoprecipitated misfolded SOD1 together with KAP3 (Fig. 5A). To visualize the misfolded SOD1-KAP3 association in PNG3 cells, we performed immunocytochemical analysis for localization of KAP3 and mutant SOD1. We found mutant SOD1-immunoreactive aggregates were prominent in cell bodies as well as the processes of MG132-treated differentiated PNG3 cells expressing G85R SOD1, and those aggregates were also positive for KAP3 (Fig. 5B and C). These observations together suggest that the cellular FALS model that we developed here using PNG3 cells recapitulates the association of KAP3 and misfolded SOD1 observed in *SOD1*^{G93A}-Tg mice and therefore is suitable to analyze the pathological impact of the misfolded SOD1-KAP3 association on motor neurons.

Microtubule-dependent fraction of depolarization-induced ACh release from PNG3 cells requires KAP3

In *Drosophila* neurons, the kinesin-2 motor complex is responsible for anterograde axonal transport of ChAT (18,19). To examine whether the same is true in mammals, we first developed an assay model to detect a depolarization-induced microtubule-dependent release of ACh as a result of ChAT transport. Differentiated PNG3 cells were metabolically

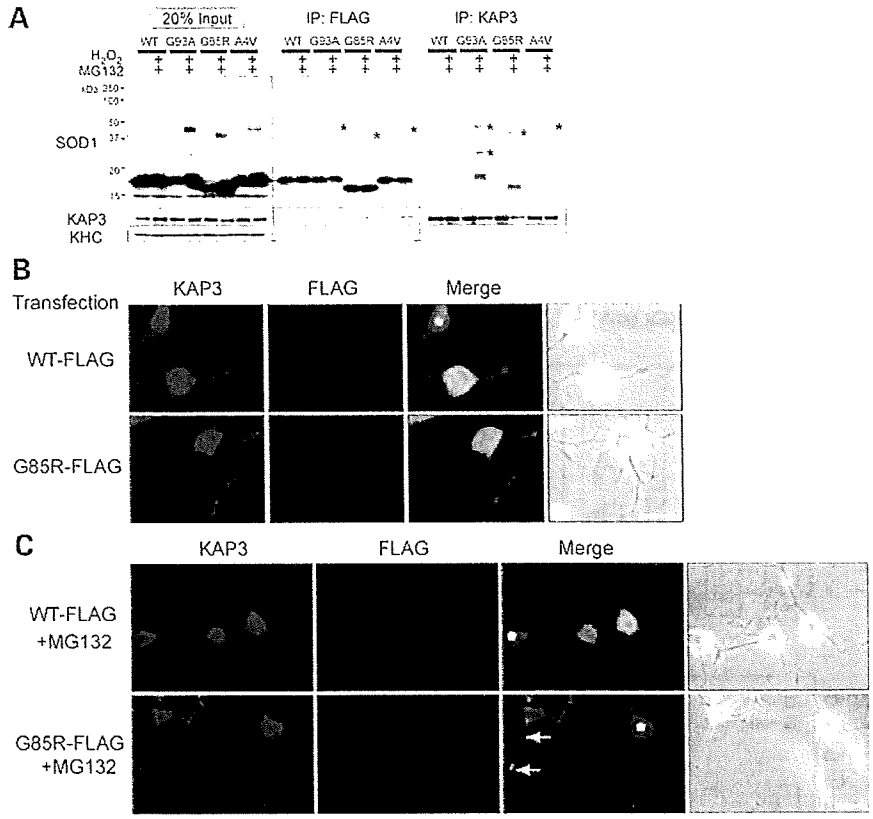

Figure 5. KAP3 associates with misfolded SOD1 species in differentiated PNG3 cells. (**A**) Immunoprecipitates of anti-FLAG and KAP3 antibodies (labeled as 'IP:FLAG' or 'IP:KAP3') from lysates of PNG3 cells transfected with expression plasmids for wild-type SOD1 or SOD1 with G93A, G85R or A4V mutation with or without induction of misfolding by MG132/H_2O_2 were analyzed for the presence of indicated proteins by immunoblot analysis. Immunoblot of lysates used for immunoprecipitation (20% of the amount) of the expression of the same set of proteins is also shown. Note that misfolded SOD1–KAP3 association was detected in all three mutant SOD1 transfectants (indicated by asterisks). (**B** and **C**) Photographs of KAP3 and FLAG-tagged SOD1 in differentiated PNG3 cells transfected with either FLAG-tagged wild-type SOD1 or SOD1 bearing a G85R mutation before and after MG132 treatment are shown in (B) and (C), respectively. Phase contrast images are also shown to the right of each set. Asterisks indicate untransfected cells. Note that prominent aggregate formation is only in the mutant SOD1-expressing cells and processes after MG132 treatment. Scale bars=25 μm.

labeled with [^{3}H]choline, and depolarization-induced [^{3}H]ACh release was measured. We observed that PNG3 cells released [^{3}H]ACh in a KCl dose-dependent manner (Fig. 6A). To distinguish 'nerve terminal' ACh release from exocytosis at other locations, we examined ACh release with and without colchicine, a microtubule destabilizing reagent that inhibits axonal transport (18). From ACh release experiments with different trial amounts of colchicine, we decided to use colchicine at 2.5 μM for the best differentiation of microtubule-dependent release representing the release from the terminal of differentiated PNG3 cellular processes. Treating the cells with this concentration converted nearly 20% of the tubulin from filamentous to free form in PNG3 cells (Supplementary Material, Fig. S3A). Then to analyze the involvement of KAP3/kinesin-2 in ChAT transport in the mammalian neuron using this assay system, we examined the effect of KAP3 mRNA down-regulation in differentiated PNG3 cells. Although NG108-15 cells are mouse–rat hybrid, transfection of siRNA for mouse KAP3 in PNG3 cells decreased the KAP3 protein level to ~15% after 2 days (Supplementary Material, Fig. S3B). We found that siRNA-mediated down-regulation of KAP3 significantly reduced the microtubule-dependent fraction of ACh release from PNG3 cells (Fig. 6B). This reduction in ACh release was rescued by the co-transfection of full-length human KAP3 which is not affected by the mouse siRNA we used. However, the ACh release was not rescued by the human KAP3 lacking C-terminal sequence (513–792 amino acids), which is required for the interaction with KIF3A/B (26). These results suggest that KAP3 is required for ChAT transport along microtubules and the subsequent release of ACh from nerve terminals in mammalian neurons.

As described above, we observed decreased ChAT axonal transport in *SOD1*^{G93A}-Tg mice. To examine whether misfolded SOD1 inhibits ChAT transport also in this FALS model system in culture, we measured microtubule-dependent ACh release from differentiated PNG3 cells after induced production of misfolded SOD1 species (procedure is summarized in Fig. 6C). We found that induction of SOD1 misfolding by MG132 treatment resulted in a significant decrease of microtubule-dependent ACh release from mutant SOD1-expressing PNG3, but not from wild-type SOD1-expressing cells

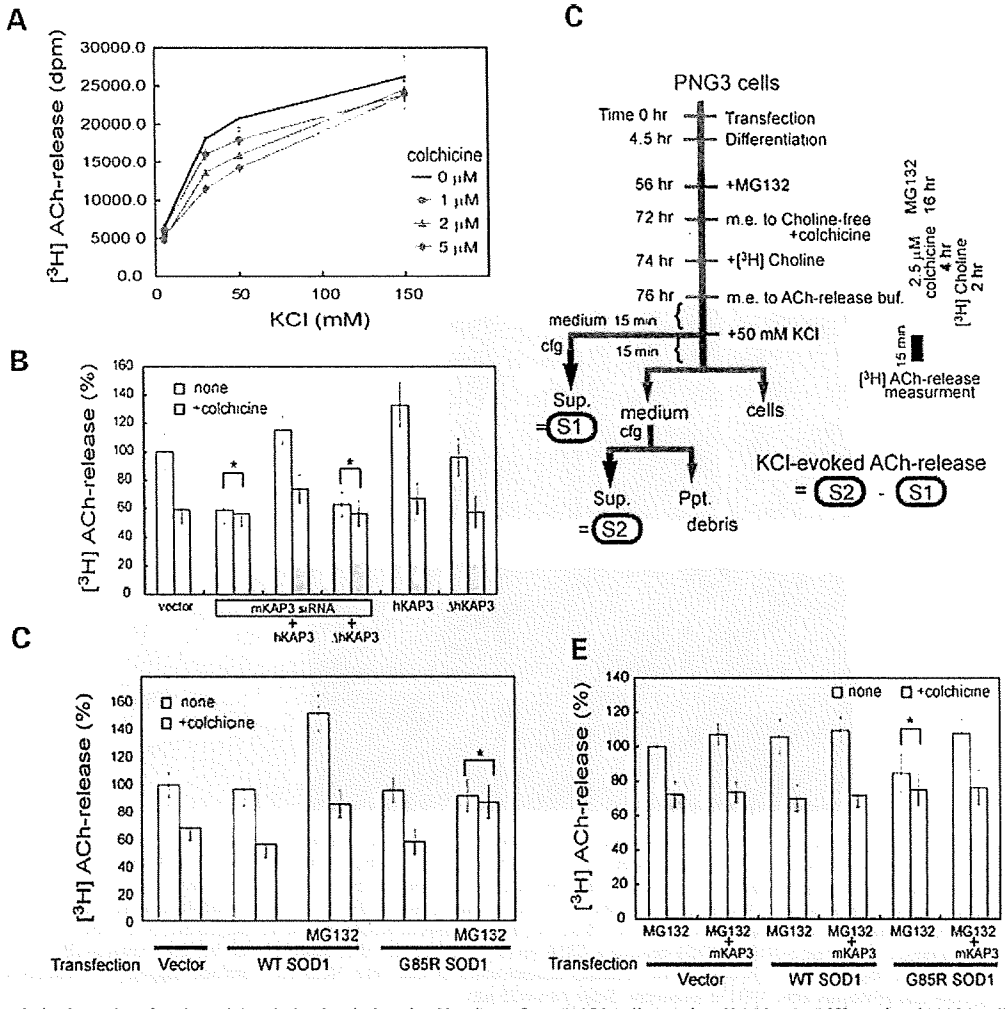

Figure 6. Microtubule-dependent fraction of depolarization-induced ACh release from PNG3 cells requires KAP3. (**A**) Differentiated PNG3 cells, metabolically labeled with [^{3}H]choline, were depolarized by increased KCl in the medium for 15 min. The radioactivity was released into the medium representing [^{3}H]ACh and was measured for different concentrations of KCl and colchicine, as indicated. (**B**) Depolarization-induced [^{3}H]ACh release from differentiated PNG3 cells transfected with vector only, siRNA for mouse KAP3 (mKAP3) or siRNA for mKAP3 together with expression plasmid for either human KAP3 (hKAP3) or hKAP3 lacking C-terminal 223 amino acids (ΔhKAP3), expression plasmid for hKAP3 only or expression plasmid for ΔhKAP3 was determined with or without colchicine treatment. Radioactivity is shown as a percentage to that from vector-transfected, colchicine-untreated cells. The asterisk indicates non-significant differences calculated as $P > 0.05$. Note that KAP3 down-regulation inhibited microtubule-dependent ACh release. (**C**) Summarized time schedule for [^{3}H]ACh-release measurement in differentiated PNG3 cells with and without SOD1 misfolding/aggregation. KCl-evoked release of ACh was calculated by subtracting the radioactivity in S1 (medium before KCl addition) from that in S2 (medium after KCl addition). (**D**) Depolarization-induced [^{3}H]ACh release from differentiated PNG3 cells transfected with vector only, expression plasmid for wild-type SOD1 or G85RSOD1 was determined with or without MG132 treatment. Microtubule-dependent and -independent fractions of release were measured for each condition analyzed. Radioactivity is shown as percentage to that from vector-transfected, colchicine-untreated cells. Note that ACh release from mutant SOD1-transfected cells was reduced in response to MG132 treatment, while overexpression of mutant SOD1 *per se* did not affect choline incorporation into cells (Supplementary Material, Fig. S4C). The asterisk indicates non-significant difference calculated as $P > 0.05$. (**E**) Depolarization-induced [^{3}H]ACh release from differentiated PNG3 cells transfected with vector only, expression plasmid for wild-type SOD1 or G85RSOD1, with or without co-transfection of mKAP3 expression plasmid, was determined after MG132 treatment. Microtubule-dependent and -independent fractions of release were measured for each condition analyzed. Radioactivity is shown as a percentage of that from vector-transfected, colchicine-untreated cells. Note that the reduction in ACh release observed in mutant SOD1-transfected cells in response to MG132 treatment was normalized by mKAP3 expression. The asterisk indicates non-significant difference calculated as $P > 0.05$.

(Fig. 6D, asterisk). MG132 treatment itself resulted in up-regulation of both microtubule-dependent and -independent ACh release (Fig. 6D and Supplementary Material, Fig. S4A). However, this MG132-induced increase in ACh release was presumably caused by increased expression levels of proteins necessary for ACh synthesis/release and was independent from the misfolded SOD1-induced effect (Supplementary Material, Figs S4B and C). These results suggest that misfolded SOD1 inhibits ChAT transport in this FALS model system in culture as well.

The observations in *SOD1*^{G93A}-Tg mice, as well as in the cellular FALS model system that we described, further

suggest that misfolded SOD1 causes a reduction or depletion of the functional kinesin-2 complex via its association with KAP3. This raises the possibility that misfolded SOD1-induced reduction in ChAT transport may be normalized by supplementing motor neurons with KAP3. To prove this hypothesis using the FALS culture model system, we examined microtubule-dependent ACh release from differentiated PNG3 cells overexpressing wild-type or mutant SOD1 together with KAP3. Overexpression of KAP3 did not change ACh release from MG132-treated PNG cells transfected with empty vector or wild-type SOD1. However, overexpression of KAP3 was able to normalize the ACh release reduction under the condition that causes mutant SOD1 misfolding (Fig. 6E). These results strongly suggest that misfolded SOD1-induced reduction in ChAT transport and ACh release is mediated by a reduction in functional KAP3 molecule because of its association with misfolded SOD1. These results may also suggest that the normalization of functional KAP3 level in motor neurons could have a therapeutic effect on FALS pathogenesis.

KAP3 was co-localized with mutant SOD1 aggregates within LBHI in spinal motor neurons from human FALS patients

As described, we performed analysis of the misfolded SOD1-induced reduction of ChAT transport in cultured cells in cultured cells as well as in a mouse model. To gain insight into the significance of this mechanism in human FALS, we performed immunohistochemistry on spinal cord sections of human SOD1-linked FALS cases to examine co-localization of KAP3 and SOD1. The neuropathological phenotypes of four patients we analyzed, who were members of two different families (27–29), are summarized in a table in Figure 7. These patients often developed Lewy-body-like hyaline inclusions (LBHIs), which are protein aggregates containing mutant/wild-type SOD1 and one of the most characteristic cytopathological changes in the spinal motor neurons of mutant *sod1*-linked FALS (28). Immunohistochemical analysis revealed that most of the LBHIs in the spinal motor neurons were positive for both KAP3 and SOD1 (arrowheads in Fig. 7). We confirmed that the KAP3 signal in LBHIs was not present when the anti-KAP3 antibody was pre-incubated with an excess of the synthetic KAP3 antigen peptides (data not shown). These observations demonstrated that KAP3–SOD1 interaction and subsequent co-aggregation frequently occurs in human SOD1-linked FALS cases.

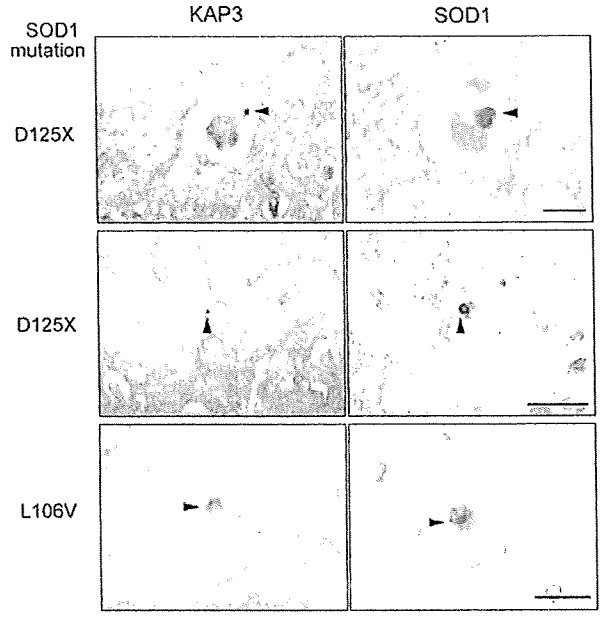

Neuropathological findings in autopsied patients with FALS examined.

SOD1 mutation	Number of patients	Neuronal inclusion	SOD1 aggregation	Bunina body	Corticospinal tract involvement	Posterior column involvement
D125X	2	LBHI	+	-	+	+
L106V	2	LBHI	+	-	+	+

+ present, - absent, LBHI: Lewy-body-like hyaline inclusion

Figure 7. KAP3 was co-localized with SOD1 aggregates within LBHI in spinal motor neurons from human FALS cases. Consecutive sections of LBHI-containing spinal motor neurons from FALS patients possessing *sod1* mutations were immunostained with anti-KAP3 and anti-SOD1 antibodies. The clinicopathological characteristics of the FALS patients are summarized in the table. D125X mutation is a deletion of two nucleotides at codon 126 that results in the truncation of five residues downstream. Co-localization of KAP3 and SOD1 within the LBHI is evident (arrowheads). The images are representative of 30 LBHIs observed in each case, all of which showed co-localization of SOD1 and KAP3. Scale bars=25 μm for the images of top row, 50 μm in others.

DISCUSSION

In this paper, we presented a novel pathological mechanism by which misfolded SOD1 may cause neuronal dysfunction in FALS. A significant proportion of misfolded SOD1 is located within motor axons prior to disease onset in *SOD1*^{G93A}-Tg FALS model mice. We showed that misfolded SOD1 species selectively binds to KAP3 (Fig. 2B and C) and that this binding may be a cause for the reduction in functional KAP3 molecule required for kinesin-2-dependent transport within motor axons (Fig. 3A and B). The kinesin-2 motor complex is particularly important, because it is required for ChAT transport (19). Decreased ChAT expression and resultant decrease in ACh release from motor nerve ends can lead to dysfunction of motor synapses at axon terminals (30,31). By employing a newly developed cell culture model of FALS, we showed that ACh release from nerve terminals was decreased presumably due to a reduction in ChAT transport resulting from KAP3 sequestration by misfolded SOD1 species (Figs 5A and C and 6D). The pathological mechanism we propose from our data is schematized in Figure 8.

ALS-like motor neuron pathology is observed in transgenic mice expressing C-terminal truncated SOD1 (L126Z), in which the mutant SOD1 expression was not clearly observed in sciatic nerve (32). This suggests that KAP3-misfolded SOD1 association is formed mostly in motor neuron cell bodies. Indeed, we detected KAP3-misfolded SOD1 associ-

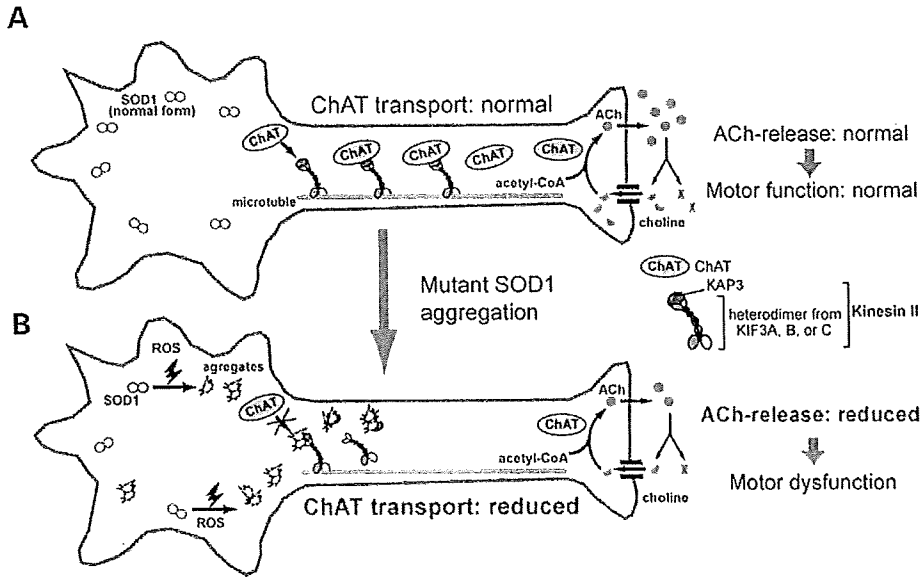

Figure 8. A schematic diagram for a mutant SOD1 toxicity and impairment of axonal transport of ChAT. In healthy motor neurons (**A**), ChAT is continuously transported by kinesin-2 motor, comprising KIF3A, KIF3B/C and KAP3, toward the neuromuscular junction where ACh functions as a neurotransmitter. ACh is released into the synaptic cleft upon stimulation and rapidly degraded into choline and acetic acid by AChE. Choline is taken up into the nerve terminal by choline transporters and then ChAT synthesizes ACh from choline and acetyl-CoA. The reaction catalized by ChAT is the rate-limiting step for ACh supply to the nerve terminals. In motor neurons expressing mutant SOD1 (**B**), mutant SOD1 proteins were converted into misfolded forms as a result of increased ROS generation and/or reduced proteasomal activity. Certain misfolded species preferentially binds to KAP3 and inhibit the binding of ChAT to KAP3, thereby causing a decrease in ChAT transport. This decrease in ChAT in the nerve terminals can constitute a mechanism that causes motor dysfunction.

ation in spinal cords (Fig. 2C) and ventral white matter (Fig. 2A and B) of *SOD1*^{G93A}-Tg mice prior to disease onset, but could not detect it in distal sciatic nerve even at the end-stage (data not shown). These findings suggest that, even if misfolded SOD1 associates with molecular motors, it cannot travel for a long distance, presumably because it is not a physiological cargo.

We suspect that misfolded SOD1–KAP3 association is one of the early events in FALS pathogenesis. Evidence to support this possibility is that the SOD1–KAP3 association becomes detectable around 6 months of age in *SOD1*^{G93A}-Tg mice, 2 months earlier than disease onset (Fig. 2C), suggesting that the SOD1–KAP3 association constitutes an early event in FALS motor neurons. Also, our immunoprecipitation/immunoblot analysis shows that SOD1–KAP3 association always detected relatively low molecular-weight misfolded SOD1 (−50 kDa) among all of the misfolded products ranging up to hundreds of kilodaltons in size (Figs 2B and C and 5A). The preferential association of KAP3 for low molecular-weight species but not with large precipitates suggests that SOD1–KAP3 association accounts for a fraction of the initial events in FALS pathogenesis. Previous reports on selective increase in KAP3 transcription in lumbar spinal cords from *SOD1*^{G86R}-Tg mice as an early event prior to disease onset (33) also supports our hypothesis, as the increase may be regarded as compensatory to the KAP3 sequestration by SOD1–KAP3 association.

Previous reports show that crossing mutant SOD1-Tg mice with dynein heavy chain mutant mice (*loa* or *cra*) delays the disease onset and extends survival (34,35). This result is surprising because mutations in dynein heavy chain, a subunit of dynein motor complex, or p150^{Glued}, a subunit of dynactin (dynein activator) cause dysfunction and degeneration of spinal motor neurons (15,16). This suggests a possible mechanistic link between impaired axonal transport in mutant *SOD1*-Tg mice and that in dynein heavy chain mutant mice. Here we demonstrated that KAP3 sequestration by misfolded SOD1 is a mechanism for selective inhibition of axonal transport observed in mutant SOD1-Tg mice. Previous reports on melanophore transport in *Xenopus* melanosomes showed that dynactin serves as an activator of kinesin-2 via direct binding of p150^{Glued} to KAP3 and regulates the intracellular direction of melanosome transport by binding to either dynein (retrograde) or KAP3 (anterograde) (36). Dynein and KAP3 share the same binding site on p150^{Glued}, and so p150^{Glued} binds to only one of them at a time and thereby activates transport in only one direction. If a similar regulation by dynactin plays a role in mammalian neurons, *loa* and *cra* mutations may increase the chance of p150^{Glued} to bind to KAP3, because those mutations promote subunit disassembly and increase dynein-unbound dynactin (15). By this mechanism, dynein heavy chain mutations may result in normalizing kinesin-2-mediated transport of ChAT inhibited by the misfolded SOD1 species. Indeed, in our analysis of ventral white matter in *SOD1*^{G93A}-Tg mice using Nycodenz density gradient centrifugation, a small fraction of p150^{Glued} co-migrated with misfolded SOD1 species and KAP3 (Fig. 2A). This population of p150^{Glued} also co-precipitated with KAP3 (data not shown). This result may reflect an involvement of p150^{Glued} in KAP3/SOD1 misfolding and aggregation through its interaction with KAP3.